A New Xantphos-type Ligand and its Gold(I) Complexes: Synthesis, Structure, Luminescence

Gábor Besenyei[a], István Bitter[b], László Párkányi[c], Gábor Szalontai[d], Péter Baranyai[a], Éva Kunsági-Máté[e], Ferenc Faigl [b], Alajos Grün[b], Miklós Kubinyi[a,e*]

[a] Institute of Molecular Pharmacology, Research Centre for Natural Sciences, Hungarian Academy of Sciences, 1525 Budapest, Pusztaszeri út 59-67, Hungary

[b] MTA-BME Organic Chemical Technology Research Group, Department of Organic Chemistry and Technology, Budapest University of Technology and Economics, 1111 Budapest, Műegyetem rkp. 3., Hungary

[c] Institute of Organic Chemistry, Research Centre for Natural Sciences, Hungarian Academy of Sciences, 1525 Budapest, Pusztaszeri út 59-67, Hungary

[d] University of Pannónia, NMR Laboratory, 8200 Veszprém, Egyetem u. 10., Hungary

[e] Department of Physical Chemistry and Materials Science, Budapest University of Technology and Economics, 1111 Budapest, Műegyetem rkp. 3., Hungary

[*] Corresponding author. Tel.: +36-1-438-1120; fax: +36-1-438-1143
Email address: kubinyi.miklos@ttk.mta.hu

ABSTRACT

A novel xantphos analogue diphosphine ligand, 9,9-dimethyl-4,5-bis(diphenylphosphinomethyl)-*9H*-xanthene ($X(CP)_2$), with methylene groups inserted between the xanthene skeleton and the two diphenylphosphine units has been synthesized. A two-coordinate and a three-coordinate gold(I) complex of the ligand, $[Au_2Cl_2(X(CP)_2)]$ and $[AuCl(X(CP)_2)]$, have been prepared and studied by X-ray diffraction, NMR and optical spectroscopy. In the solid state, $[AuCl(X(CP)_2)]$ adopts a highly ordered structure with a planar xanthene skeleton that faces another plane composed of two phenyl rings and the AuCl moiety. The structure of $[Au_2Cl_2(X(CP)_2)]$ is much less regular, the two P-Au-Cl vectors show to the opposite sides of the folded xanthene backbone. The exchange-broadened resonances in the NMR spectra of $[AuCl(X(CP)_2))]$ indicate that this complex exists as a mixture of various chemical species and/or conformers in solution. In contrast, the NMR spectra of $[Au_2Cl_2(X(CP)_2)]$ exclude any medium-range exchange processes. Aurophilic interactions are absent in both $X(CP)_2$ complexes. $X(CP)_2$ as well as its two gold complexes are phosphorescent in solid state, the complexes emit at higher wavelengths and with longer lifetimes than the free ligand.

Keywords:
gold(I) complexes
phosphine ligands
coordination modes
crystal structure
luminescence

1. Introduction

4,5-bis(diphenylphosphino)-9,9-dimethyl-*9H*-xanthene (xantphos; XP_2 in Scheme 1), synthesized first by Kranenburg et al. [1] and Hillebrand et al. [2], has been applied as a phosphine ligand in the preparation of a great number of transition metal complexes. The xanthene skeleton is not fully rigid [3,4], the dihedral angle characterizing its folding and the torsion angle characterizing its twisting, and thereby the P···P distance and the P-M-P chelating angle vary in xantphos complexes, depending on the central metal atom and the counter ligands [5]. This explains the structural variety of xantphos complexes, demonstrated by studies on its Pd [6], Pt [7], Rh [5] and Ir [8] complexes, in which it acts as a monodentate, a bidentate (P,P with *cis* or *trans* coordination mode) or a tridentate (P,O,P) ligand. Many of its Pd, Ru, Rh complexes proved to be efficient catalysts in homogeneous catalytic reactions [9,10]. Combined X-ray and catalytic studies on the complexes of xantphos and other diphosphines revealed that the catalytic effect depends on the P-M-P 'bite angle' [6,11,12].

Xantphos is also an important ligand in gold chemistry: it can form dinuclear complexes with intramolecular aurophilic interactions [4,13,14,15,16]. In addition, a three-coordinate [17] and a four-coordinate [13] (quasi tetrahedral) gold(I) xantphos complex have also been reported, with lack of aurophilic interaction.

Many of the organometallic complexes with diphosphine ligands exhibit a strong luminescence at room temperature, making them attractive candidates as indicators in optical sensors and as emitters in electroluminescent devices [18,19]. Xantphos occurs as a diphosphine ligand in luminescent Cu(I) [20,21,22] and Au(I) [4,13,14,23,24] complexes. The quenching of luminescence of Cu(I) xantphos complexes by oxygen was utilized for constructing optical sensors [21]. Heteroleptic Cu(I) complexes with a xantphos and a pyrrole derivative ligand have been tested as emitting layers in LED devices [22]. Au(I) xantphos complexes can also be expected to show photophysical properties interesting for such technical applications, in particular that gold complexes with aurophilic interactions have special luminescence characteristics [25,26].

Scheme 1 here

In order to gain further information on the effects of the ligand flexibility on the properties of diphosphine complexes, in the present work a new diphosphine ligand with

xanthene skeleton, 9,9-dimethyl-4,5-bis(diphenylphosphinomethyl)-*9H*-xanthene ($X(CP)_2$ in Scheme 1), has been prepared, in which the diphenyphosphine units and the xanthene scaffold are separated by methylene groups, and two gold(I) complexes of the new ligand – $[AuCl(X(CP)_2)]$ and $[Au_2Cl_2(X(CP)_2)]$ - have been prepared and studied by X-ray diffraction, NMR and luminescence spectroscopy.

2. Materials and methods

The reagents used in the syntheses were purchased from Aldrich and used without purification. Hexane was distilled from P_2O_5. All moisture or air sensitive compounds were synthesized under a nitrogen atmosphere using standard Schlenk techniques. For column chromatography Merck Kieselgel 60 (0.063-0.20 mm), for analytical TLC Merck Kieselgel GF_{254} were used.

2.1. Synthesis

*2.1.1. 9,9-Dimethyl-9H-xanthene-4,5-dicarbaldehyde (**1**)*

9,9-Dimethyl-*9H*-xanthene (5.0 g, 23.8 mmol) was dissolved in dry hexane (160 cm^3) under an inert nitrogene atmosphere and *N,N,N'N'*-tetramethylethylenediamine (TMEDA, 6.9 g, 8.9 cm^3, 59.5 mmol) was added into it at 25 ^oC. A solution of butyllithium in hexane (1.59 mol/dm^3, 38.0 cm^3, 59.5 mmol) was added dropwise to the stirred reaction mixture while a dark red solution was formed. It was refluxed for 30 minutes, then cooled down to 25 ^oC before dry *N,N*-dimethyl-formamide (4.4 g, 5.0 cm^3, 60.2 mmol) was poured into the reaction mixture. The dark solution was stirred for 1 hour while its colour became yellow. Aqueous hydrochloric acid (2 mol/dm^3, 150 cm^3) was added and the mixture was stirred for 15 minutes. The precipitate was filtered off, washed with water (2×20 cm^3) then with hexane/ethyl acetate = 9/1 mixture (2×20 cm^3) and dried to yield the titled compound as an off-white solide (5.8 g, 91%), TLC R_F: 0.25, eluent hexane/ethyl acetate = 9/1. An analytically pure sample were obtained by recrystallization of the crude product from ethyl acetate.

^{1}H NMR: δ 10.69 (2H, s, C*H*O), 7.81 (2H, dd, *J* 7.6, 1.6, Ar*H*), 7.71 (2H, dd, *J* 7.8, 1.6, Ar*H*), 7.26 (2H, t, *J* 7.6, Ar*H*), 1.70 (6H, s, CH_3).[†]

Note: 9,9-Dimethyl-*9H*-xanthene-4,5-dicarbaldehyde is known from the literature. Dilithiation of 9,9-dimethyl-*9H*-xanthene followed by DMF addition was accomplished first with 3 equivalents of butyllithium/TMEDA mixture in diethyl ether/hexane solution [27] to provide the target compound in 72% yield. Similar yield was achieved when the reaction sequence was carried out in a tetrahydrofuran/hexane mixture and the crude product was purified by column chromatography [28].

Modification of the above mentioned methods allowed to provide the desired product in much higher yield. Actually, dimetalation was carried out in pure hexane at reflux temperature followed by the addition of DMF at room temperature and a simple aqueous hydrolysis. Under these conditions the product precipitated from the reaction mixture in 91% yield and it could be used in the next reactions without any purification.

[†] Abbreviations used in the description of the NMR spectra are s, singlet; d, doublet; m, multiplet; t, triplet; p.q., pseudo quintet; p.t., pseudo triplet; br, broad.

*2.1.2. 4,5-bis(Hydroxymethyl)-9,9-dimethyl-9H-xanthene (**2**)*

To the EtOH solution (60 cm^3) of dialdehyde **1** (2.75 g, 10.4 mmol) was added $NaBH_4$ (2.6 g, 70 mmol) and stirred overnight at ambient temperature. The mixture was then evaporated to dryness, treated with water (50 cm^3) and acidified with dilute HCl followed by extraction with ethyl acetate (2x50 cm^3). The combined organic phases were washed with water (50 cm^3), dried (Na_2SO_4) and the volatiles were removed under reduced pressure. The product was crystallized with ether to obtain 2.4 g (86%) white semi-solid in essentially pure form. TLC: R_F 0.35 (toluene-MeOH = 8:2).

^{1}H NMR: δ 7.38 (dd, 2H, *J* = 8 Hz, 1.5 Hz, Ar*H*), 7.14 (dd, 2H, *J* = 7 Hz, 1 Hz, Ar*H*), 7.04 (t, 2H, *J* = 7.5 Hz, Ar*H*), 4.73 (s, 4H, CH_2), 1.62 (s, 6H, CH_3);.^{13}C NMR δ 149.0, 130.5, 128.1, 127.9, 126.2, 123.1 (Ar), 62.1(*C*H_2), 34.3 (*C*), 32.3 (*C*H_3)

*2.1.3. 4,5-bis(Bromomethyl)-9,9-dimethyl-9H-xanthene (**3**)*

To the $CHCl_3$ solution (30 cm^3) of diol **2** (2.0 g, 7.4 mmol) was dropped PBr_3 (1.75 cm^3, 18 mmol) dissolved in $CHCl_3$ (10 cm^3) and stirred for 2 h at ambient temperature. Then saturated aqueous $NaHCO_3$ solution (60 cm^3) was added carefully, the organic phase was separated, washed with water (2x50 cm^3), dried (Na_2SO_4) and evaporated to obtain 2.55g (87%) white semi-solid. TLC: R_F 0.75 (hexane-EtOAc = 8:2).

^{1}H NMR δ 7.40 (dd, 2H, *J* = 7.5 Hz, 1 Hz, Ar*H*), 7.27 (dd, 2H, *J* = 7.5 Hz, 1.5 Hz, Ar*H*), 7.07 (t, 2H, *J* = 8 Hz, Ar*H*), 4.82 (s, 4H, CH_2), 1.63 (s, 6H, CH_3);.^{13}C NMR δ 147.9, 130.2, 128.8, 127.0, 125.3, 123.2 (Ar), 34.2, (*C*), 32.5 (*C*H_3), 28.8 (*C*H_2Br)

*2.1.4. 9,9-Dimethyl-4,5-bis(diphenylphosphinoylmethyl)-9H-xanthene (X(CPO)$_2$, **4**)*

Dibromide **3** (1.58 g, 4 mmol) was dissolved in THF (10 cm^3) and dropped into potassium diphenylphosphide solution (0.5 M, 21 cm^3). The mixture was refluxed for 12 h, then the solvent was evaporated in vacuo. The residue was dissolved in $CHCl_3$ (70 cm^3), washed with water and chilled, then 30% H_2O_2 (5 cm^3) was added to complete the oxidation. After standard work-up the product was purified by column chromatography (eluent: toluene-methanol = 9:1) to yield 1,1g (43%) white solid. Mp>230 ^{o}C. Anal. cacd. for $C_{41}H_{36}O_3P_2$ (**4**): C 77.10, H 5.68; found C 76.76, H 5.83.

^{1}H NMR ($CDCl_3$): δ 7.68-7.60 (m, 8H), 7.43-7.37 (m, 4H), 7.33-7.26 (m, 8H), 7.21-7.17 (m, 2H), 7.08-7.04 (m, 2H), 6.94-6.89 (m, 2H), 3.75 (d, 4H, $^2J_{HP}$ = 14.5 Hz, CH_2), 1.40 (s, 6H, CH_3); ^{31}P NMR ($CDCl_3$, 161.97 MHz): 30.4 ppm (s); ^{13}C NMR ($CDCl_3$, 100.6 MHz, (see Scheme 2): 148.1, (d, 5.6 Hz, C1), 133.0 (d, $^1J_{PC}$ = 98 Hz, C10), 131.6 (d, 2.6 Hz, C13), 131.1 (d, $^2J_{PC}$ = 8.8 Hz, C11), 130,2 (d, 2.5 Hz, C2), 129.4 (d, 4.5 Hz, C5), 128.3 (d, 11.6 Hz, C12), 124.3 (d, 3.2 Hz, C3), 122.8 (d, 2.8 Hz, C4), 118.9 (d, 8.0 Hz, C6), 34.2 (s, C8), 31.9 (d, $^1J_{PC}$ = 68.0 Hz, C7), 31.4 (s, C9).

Scheme 2 here

Note: During the reaction the majority of phosphine formed became oxidized to phosphine oxide, therefore the product mixture was treated with H_2O_2 to achieve complete oxidation.

*2.1.5. 9,9-dimethyl-4,5-bis(diphenylphosphynylmethyl)-9H-xanthene, (X(CP)$_2$, **5**)*

Of the various routes suitable to convert phosphine oxides to phosphines that suggested in Ref. [29] was followed. A suspension of 0.38 g (0.60 mmol) of **4** in 25 cm^3 of toluene and 6 cm^3 of triethylamine was cooled to 0°C. 2.01 g (14.9 mmol) of $HSiCl_3$ was added under N_2 and the reaction mixture was thermostated at 95°C for 22 hours. The pale yellow slurry was cooled to 0°C and a solution of 5.0 g of NaOH in 20 cm^3 of H_2O was

introduced from a syringe. The reaction mixture was allowed to warm to ambient temperature then was further heated at 45°C until all the white precipitate in the bottom (water) phase dissolved (ca. 45 min.). To the two-phase mixture, 55 cm^3 of diethyl ether was added and the upper (organic) phase was transferred into a flask containing $MgSO_4$. The drying agent was separated by filtration and the solvent mixture was removed under reduced pressure to give a pale yellow oil that slowly solidified on standing. Recrystallization of the crude product from methanol yielded 228 mg (62.6%) of pure diphosphine, Evaporation of the mother liquor to ca. 2 cm^3 allowed the isolation of a second crop (36 mg, 10%) of the target compound. Anal. cacd. for $C_{41}H_{36}OP_2$ (**5**): C 81.17, H 5.98; found 80.79, H 6.00.

^{1}H NMR ($CDCl_3$): 7.34-7.19 (overlapping multiplets, 22H), 6.89-6.85 (m, 2H), 6.75-6.70 ppm (m, 2H), 3.58 (s, 4H, CH_2), 1.60 (s, 6H, CH3); ^{31}P NMR ($CDCl_3$, 161.97 MHz): −13.1 ppm (s); ^{13}C NMR ($CDCl_3$, 100.6 MHz, (see Scheme 2): 148.3, (p.t., C1), 138.6 (d, $^1J_{PC}$ = 15.2 Hz, C10), 132.9 (d, $^2J_{PC}$ = 18.5 Hz, C11), 130,1 (p.t., C2), 128.8 (p.t., C5), 128.4 (s, C13), 128.2 (p.t., C12), 124.6 (p.t, C6), 123.4 (p.t. C3), 122.3 (p.t., C4), 34.3 (s, C8), 31.8 (s, C9), 29.7 (p.q., C7).

*2.1.6. [AuCl(X(CP)$_2$)], (**6**)*

Into a solution of 63.5 mg (0.105 mmol) of **5** in 5 cm^3 deoxygenated CH_2Cl_2, 33.5 mg (0.105 mmol) of [AuCl(tht)] [30] was added and the reaction mixture was stirred for 30 min. The solution was then concentrated to ca. 2 cm^3. Addition of 10 cm^3 of ethyl ether and further stirring for an additional 60 min resulted in white powder that was collected on a glass filter, washed with ethyl ether and dried under vacuum. Yield: 66 mg (75%). Crystals isolated upon diffusion of diethyl ether vapors into a CH_2Cl_2 solution of **6** were suitable for crystallographic studies. Anal. cacd. for $C_{41}H_{36}ClOP_2Au$ (**6**): calcd. C 58.69, H 4.32; found C 58.38, H 4.36.

^{1}H NMR (CD_2Cl_2): 7.36-7.22 (om, 6H), 7.15-7.00 (unresolved, 16H), 6.76-6.68 (m, 2H), 6.46-6.38 (unresolved, 2H), 3.84 (br, s, 4H, CH_2), 1.56 (s, 6H, CH_3); ^{31}P NMR(CD_2Cl_2): 32.6 ppm (br, s).

2.1.7. [Au$_2$Cl$_2$(X(CP)$_2$)], (7)

A mixture of 32,0 mg (0.053 mmol) of diphosphine **5** and 33.8 mg (0.105 mmol) of [AuCl(tht)] was dissolved in 6 cm^3 of deaerated dichloromethane and stirred at RT for 15 min under N_2. The solution was concentrated to ca. 2 cm^3 under reduced pressure and methanol (8 cm^3) was added in small portions. The white precipitate formed was filtered off, washed with methanol and dried under vacuum.Yield: 43 mg (76%). Crystals suitable for crystallographic studies were obtained by diffusion of vapors of diethyl ether into an acetonitrile solution of the target compound. Anal. cacd. for $C_{41}H_{36}Cl_2OP_2Au_2$ (**7**): calcd. C 45.96, H 3.39; found C 45.50, H 3.43.

^{1}H NMR ($CDCl_3$): 7.60-7.49 (m, 8H), 7.49-7.42 (m, 4H), 7.38-7.28 (m, 10H), 6.86-6.78 (m, 2H), 6.48-6.42 (m, 2H), 4.03 (d, $^2J_{HP}$ = 11.8 Hz, 4H, CH_2), 1.60 (s, 6H, CH_3); ^{31}P NMR ($CDCl_3$): 28.5 ppm (s).

2.2. X-ray diffraction

Intensity data were collected on a Rigaku Rapid IP diffractometer with Mo-*Kα* radiation (λ = 0.71075 Å) at 293 K. Numerical absorption corrections were applied in all cases. The structures were solved by direct methods and refined [31] with anisotropic least-squares for the non-hydrogen atoms. Hydrogen atomic positions were generated from assumed geometries and were not refined.

2.3. NMR spectroscopy

NMR spectra were recorded on a Bruker Avance DRX 500 and a Bruker Avance II 400 instrument using tetramethylsilane (^{1}H, ^{13}C) as internal standard and 85% H_3PO_4 (^{31}P) as external standard, in $CDCl_3$ or CD_2Cl_2 solutions.

2.4. Optical spectroscopy

The UV absorption spectra were recorded on an Agilent 8453 diode array spectrometer. The fluorescence and phosphorescence measurements were carried out on an Edinburgh Instruments FLSP920 fluorescence and phosphorescence lifetime and steady state spectrometer. The excitation light source was a Xe900 steady state xenon arc lamp, when measuring the fluorescence spectra, a nF900 nanosecond flashlamp filled with hydrogen gas, when the fluorescence decay curves measured and a μF900H microsecond xenon flashlamp, when the phosphorescence spectra and decay curves were recorded.

3. Results and Discussion

3.1. Synthesis

Scheme 3 here

The sequence of reaction steps is summarized in Scheme 3. The ligand ($X(CP)_2$), **5**, was obtained via a multistep synthesis starting from 9,9-dimethyl-*9H*-xanthene. In the first reaction selective deprotonation of the xanthene backbone in the positions 4 and 5 (activated by the heteroatom) [1,2], was accomplished by 2.5 equiv. of *n*-BuLi/TMEDA in hexane. The dilithiated species was reacted with *N,N*-dimethylformamide followed by an aqueous hydrolysis affording the 4,5-bis(aldehyde) intermediate **1** in high (>90%) yield. Further treatment with $NaBH_4$ in ethanolic medium followed by acidification converted **1** to 4,5-bis(hydroxymethyl)xanthene **2** which, in turn, was transformed to 4,5-bis(bromomethyl)-9,9-dimethyl-*9H*-xanthene **3** with PBr_3 as brominating agent. Exchange of the bromine atoms for Ph_2P moieties was achieved by condensing **3** with $KPPh_2$ in THF. Unfortunately, the target diphosphine appeared only as a minor constituent of the reaction mixture, in which the bis(phosphine oxide) **4**, and the corresponding phosphine monoxide could be identified as major components. In order to facilitate the spectroscopic characterization of the isolated product and also to supply a uniform starting material for the next reaction step, the mixture of the isolated products was oxidized by H_2O_2 to bis(phosphine oxide). Finally, a mixture composed of $HSiCl_3$ and Et_3N in toluene was used to convert **4** to the target diphosphine 9,9-dimethyl-4,5-bis(diphenylphosphinomethyl)-*9H*-xanthene **5**.

The mononuclear [$AuCl(X(CP)_2)$], **6**, and dinuclear [$Au_2Cl_2(X(CP)_2)$], **7**, complexes of the novel $X(CP)_2$ ligand were prepared then via the interaction of the diphosphine ligand

with [AuCl(tht)] (tht stands for tetrahydrothiophene) supplying the reagents in 1:1 or 1:2 molar ratio.

To our knowledge, not only the target diphosphine but also the intermediates **2**-**4** are novel compounds, whose spectroscopic data are given in section Materials and methods.

3.2. Crystal structures

Besides the structures of the two Au complexes of $X(CP)_2$, the structure of the oxidized ligand, $X(CPO)_2$ has also been determined by X-ray diffraction. Crystals of $X(CP)_2$, suitable for such measurements could not be obtained. The unit cell, data collection and refinement parameters for $X(CPO)_2$, $[AuCl(X(CP)_2)]$ and $[Au_2Cl_2(X(CP)_2)]$ are presented in Table 1.

Table 1 here

The molecular structure of $X(CPO)_2$ is presented in Fig. 1, selected metric parameters for this molecule are collected in Table S1 in Supporting Information. The oxidized ligand crystallizes without the inclusion of solvent molecules. While the basic structural data, such as C-C, C-P and P-O bond lengths as well as the bond angles do not show any peculiarities, the planar conformation of the xanthene moiety, and the extensive (intra- and intermolecular) hydrogen bond network (Table 2) deserve attention.

Fig. 1 here

Fig. 2 here

Table 2 here

The most striking structural feature of $X(CPO)_2$ is the almost perfect coplanarity of the three-ring system of the xanthene fragment. While the angles formed by the planes of the two aromatic rings in the closely related structure of xantphos [2] are 23.4° (XP_2), 20.1° (XP_2.THF), and from slight to moderate tilting can also be observed in the oxidized form of this diphosphine, ($X(PO)_2$ [32], 31.1, 30.1 and 11.4°), the respective angle is only 3.1° in $X(CPO)_2$. The variations of this dihedral angle prompted us to search the Cambridge Crystallographic Database and 403 dimethylxanthene moietes were retrieved. It is worth to note that crystal structure of dimethyl (or diethyl) xanthene has not been reported. The distribution of the phenyl dihedral angles are shown in Fig. S1. Values distribute over a range

from 0 to 50.4° testifying for the flexibility of this ring system. We believe that the remarkable difference in coplanarity can be attributed to the dissimilar arrangement of the Ph_2P units in molecules where they are directly bonded to the xanthene backbone compared to our case where this coupling is accomplished through inserted CH_2 groups. In the former group of compounds, the lone pair of electrons on the phosphorus atoms as well as the P=O fragments point toward the same side of the xanthene unit allowing thereby different intra- and intermolecular interactions to occur on the two sides of the plane. This arrangement is demonstrated in Fig. 2. The net outcome of uncompensated effects may result in bent xanthene backbones. The opposite orientation of the two P=O units in our case, however, makes the two sides of the xanthene unit to be symmetrically affected by secondary interactions, and, consequently, a coplanar arrangement of the three rings is preferred.

Fig. 3 here

Table 3 here

The three-coordinate, mononuclear nature of [AuCl(X(CP)$_2$)], was confirmed by X-ray crystallographic analysis (Fig. 3). The molecule has *Cs* symmetry, the mirror plane passes through the Au1, Cl1, O1, C7, C8 and C8a atoms (and one hydrogen atom from each methyl group). Bond distances and angles around the gold atom are presented in Table 3. As illustrated by the right view of the structure in Fig. 3, the rings of the xanthene moiety are arranged in ideal coplanarity. (The mean deviation is 0.007 Å, the largest deviations from least square-plane are O1 0.0022 Å and C7 0.019 Å.) Surprisingly, the phosphorus, gold and chlorine atoms with two of the phenyl rings also form a plane that is obviously stabilized by strong intramolecular interactions. Of these, two C-H···Cl bonds seem to make the most significant contribution (Table 2) (d(H···Cl) = 2.72 Å, φ(C-H···Cl) = 171.0° [intramolecular] and 2.75 Å, 156.0° [intermolecular]; doubled by symmetry). The two planes are linked by two P-C(H_2) bonds and imitate the form of a boat. Other short contacts are listed in Table S2. The Au···O distance is shorter by 0.08 Å than the sum of the respective contact radii and the O1···Au1 vector direction coincides with the expected lone pair orientation of the oxygen atom. In the structurally related monogold complexes [AuCl(XP_2)] and [AuCl(X(Pxyl)$_2$)], [17] the Au···O distances are longer (3.124-3.203 Å) although the phosphorus atoms are directly connected to the xanthene backbone in these structures. The methylene hydrogen atoms pointing toward the plane of symmetry establish short contacts with the oxygen atom (d(O···H) = 2.46 Å, φ(C-H···O) 98.2°; (the sum of the van der Waals radii 2.72 Å), and,

together with the Au···O interaction, may contribute to the observed stability of the monogold species. The φ(P-Au-P) angle is wider (129.50(4)°) than that in the mononuclear complexes [AuCl(XP_2)] and [AuCl(X(Pxyl)$_2$)] [17] (116.7°, 117.8 ° and 120.6°) and approaches the value found in [AuCl($Ph_3P)_2$] [33] where the two phosphorus donor atoms are not linked by a carbohydride backbone. The lengthening of the Au-Cl bond in [AuCl(X$(CP)_2$)] 2.523(2) (Å) compared to the bond distances of 2.462, 2.457 and 2.475 Å in the xantphos counterparts [AuCl(XP_2)] and [AuCl(X(Pxyl)$_2$)] is attributable to steric reasons and to some extent to hydrogen bonds established by the chlorine atoms as outlined above.

Fig. 4 here

Indeed, the Au-Cl bond distances in gold(I) complexes of the type P-Au(Cl)-P seem to depend on steric factors: the wider the P-Au-P angle is the longer the Au-Cl bond gets. 62 three-coordinate gold(I) complexes were retrieved from the Cambridge Crystallographic Database and the Au-Cl distances show a fair correlation with the P-Au-P angles (cf. Fig. 4). For some outliers other factors may contribute (*e.g.* the phosphorus atoms are part of a macrocycle). The Au-Cl distance range is 0.51 Å (2.44 - 2.95 Å), while the P-Au-P angle range is 57.4° (116.1 – 173.5°), the correlation coefficient is 0.907.

Fig. 5 here

Contrary to the strict intramolecular orderliness of the individual fragments of the monogold complex, the structure of the dinuclear [Au_2Cl_2(X$(CP)_2$)] compound, (see Fig. 5) seems to be much less regular. The molecule lacks any (even approximate) symmetry and the P-Au-Cl vectors point to opposite sides of the best plane of the xanthene moiety which is, in this case, bent by 25.8°. There seems to be no intramolecular C-H···Cl hydrogen bonds although several C-H···π interactions (2.90, 2.92 Å) can be identified. While most of the bond lengths and bond angles can be considered as normal, the Au-P and Au-Cl bonds deserve attention. The former in [Au_2Cl_2(X$(CP)_2$)] (2.231(1) Å) is noticeably shorter than the respective distance in [AuCl(X$(CP)_2$)] (2.306(1) Å). The shortening of the Au-P distance may be ascribed to the fact that the chlorine atom has a weaker *trans* influence than a phosphorus donor group. Further, the Au-Cl bond lengths in [Au_2Cl_2(X$(CP)_2$)] (2.282(1) and 2.286(1) Å) are remarkably shorter than the Au-Cl separation in [AuCl(X$(CP)_2$)] (2.523(2) Å). The significant decrease of the Au-Cl distance may be attributable to the lack of any steric

hindrance and hydrogen bonds in the dinuclear complex, which, however, dominate the environment of the chloride ligand in the monogold complex. There are 491 P-Au(dicoordinated)-Cl fragments in the CCDC data base and their distribution follow a Gaussian curve. The average Au-Cl bond is 2.288 Å (the minimum 2.233 and the maximum is 2.337 Å). The chlorine atom in $[Au_2Cl_2(X(CP)_2)]$ does not participate in any short non-bonded interactions. In the related complex $[Au_2Cl_2(XP_2)]$ [13] strong (2.9947(4) Å) Au···Au aurophilic interaction is observed. The Au-Cl bonds are slightly longer (see Table 3) and the Au-P bond distances are comparable to $[Au_2Cl_2(X(CP)_2)]$.

3.3. NMR spectra

The NMR spectra of diphosphine $X(CP)_2$ are consistent with the proposed structure. In the ^1H NMR spectrum (Fig. S2 in SI), the *ortho* and *meta* hydrogen atoms of the xanthene backbone show up separately from the rest of the aromatic protons as multiplets at 6.74 and 6.87 ppm, respectively. The methyl protons appear at 1.60 ppm as a sharp singlet while the resonance attributable to the methylene hydrogens can be observed at 3.58 ppm, apparently with no detectable two-bond coupling to the adjacent phosphorus atoms. In the $^{31}P\{^1H\}$ spectrum (Fig. S3 in SI), $X(CP)_2$ gives a sharp singlet at −13.1 ppm. The interpretation of the $^{13}C\{^1H\}$ NMR spectrum (Figs. S4 and S5 in SI) is not straightforward. While the methyl carbon atoms (C9, 31.8 ppm), the bridging quaterner carbon carrying them (C8, 34.3 ppm) and the remote *para* carbon atoms of the phenyl rings (C13, 128.4 ppm) appear as singlets, all other carbon nuclei can be observed as doublets, pseudo triplets and pseudo quintets (for numbering of C atoms see Scheme 2 in the Experimental Section). This second-order feature may be attributed to a weak coupling between the phosphorus nuclei eight bonds apart of each other. The nature of this coupling is most probably „through-space". Such through-space couplings has been identified, for example in the spectra of bis(4*R*,6*R*)-4,6-dimethyl-1,3,2-dioxaphosphorinan-2-oxy-alkane derivatives [34] or in the spectra of xantphos and its analogues [1,2]. The phenomenon was seen as a consequence of the spatial closeness of the P-atoms and their lone electron pairs (values reported for the interatomic distances are 4.045, 4.080 and 4.115 Å, see the same references). In conformity with this explanation, no *J*(P···P) was observed when the organic backbones allow (DPEphos) or force out (DBFphos, 5.760-5.956 Å) larger separations of the interacting P-nuclei [1]. Although the solid state structure of $X(CP)_2$ is not known for us at the moment, our crystallographic study on its dioxide,

$X(CPO)_2$, has revealed a P···P distance of 4.836 Å. Due to the relatively large spatial demand of the diphenylphosphino groups, it seems reasonable to suppose that the orientation of the non-bonding phosphorus electron pairs toward the central regions of the molecule is energetically more advantageous than that of the phenyl groups, and, therefore, the time averaged value of the P···P separation may still allow an observable through-space coupling to occur in solutions. Simulation of the quintet-like splitting of the C7 methylene carbon (29.7 ppm) has shown that a weak P···P coupling (1.6 Hz) is a prerequisite of the observed slightly unequal intensity of the inner and outer lines. This splitting mode was transformed into a first order doublet of doublets when *J*(P···P) was set to zero (see Fig. S6 in SI). As a further proof, no resonances other than singlets and doublets can be observed in the ^{13}C NMR spectrum of the oxidized diphosphine $X(CPO)_2$ where interaction of the phosphorus free electron pairs is not feasible.

Our NMR studies have revealed a non negligible sensitivity to aerial oxidation of $X(CP)_2$ resulting bis(phosphine oxide) through the phosphine/phosphine oxide intermediate. Therefore, all manipulations in solutions, including the potentially lengthy NMR experiments, were carried out in deoxigenated solvents under a nitrogen atmosphere, although the pure, solid diphosphine can be stored in the refrigerator for months. This feature of $X(CP)_2$ contrasts with the inertness of xantphos [1] but coincides with the behavior of the structurally related 2,11-bis(diphenylphosphinomethyl)benzo[*c*]phenanthrene, transphos [35], as both $X(CP)_2$ and transphos are formally diphenylbenzylphosphine-type compounds.

In the ^1H NMR spectrum of the oxidized diphosphine, $X(CPO)_2$ (Fig. S7 in SI) , all the chemically different aromatic protons can be observed as separate multiplets. The methylene protons are high-frequency shifted, they appear as a doublet at 3.75 ppm while the methyl hydrogens suffer an opposite shift and can be detected as a singlet at 1.40 ppm. As mentioned above, the ^{13}C NMR spectrum of $X(CPO)_2$ does not indicate any through-space coupling between the P-nuclei. (The ^{31}P and ^{13}C NMR spectra of the dioxide can be seen in Figs. S8-S10 in SI.)

Fig. 6 here

The coordination of one equivalent of AuCl to $X(CP)_2$, *i.e.* the formation of a ten-membered ring is accompanied by changes in the NMR spectra characteristic to exchange processes. Accordingly, the methylene resonance as well as the peaks originating from the aromatic hydrogen atoms are broadened in the NMR spectrum of [AuCl($X(CP)_2$)], **6**,

compared to those of $X(CP)_2$ and the dinuclear species $[Au_2Cl_2(X(CP)_2)]$, **7** (see Fig. 6, complete ^1H and ^{31}P NMR spectra of the complexes are presented in Figs. S11-S14 in SI). These features as well as the broad phosphorus resonance indicate that the locked conformation of the monogold complex observed in the solid state is not retained in solution but, instead, dynamic interconversion of various species takes place. We did not attempt to clarify the chemical nature of the individual components in this mixture. Note, however, that NMR spectroscopic studies on solutions of [AuCl(diphosphine)] complexes have led to the assumption of various equilibrium processes. Thus, with transphos ligand, the interconversion of the [AuCl(transphos)] and [Au(transphos)]Cl components could be deduced [36]. On the contrary, with the structurally more rigid xantphos diphosphine, $[Au_2Cl_2(\mu\text{-xantphos})_2]$ and [AuCl(xantphos)] constituents have been identified in a multicomponent system at AuCl:xantphos = 1:1 molar ratio [13].

The NMR spectra of the dinuclear complex $[Au_2Cl_2(X(CP)_2)]$ are consistent with the proposed structure. The sharp proton and phosphorus resonances are indicative of the absense of medium-range exchange processes. As expected, the two-bond ^{31}P-^1H coupling value changes upon complexation to the Au atoms so the methylene protons appear as a doublet (^2J(HP) = 11.8 Hz), the methyl hydrogens give a sharp singlet.

3.4. Optical spectra

The data of the absorption and phosphorescence spectra of the $X(CP)_2$ ligand and its two gold complexes are summarized in Table 4. The absorption spectra of these compounds in CH_2Cl_2 solution, and their phosphorescence spectra and phosphorescence decay curves measured in solid state are shown in Fig. 7.

Table 4 here

Fig. 7 here

The absorption spectrum of the free ligand $X(CP)_2$ involves a multicomponent band ranging to ~ 300 nm, which is associated with the $\pi \rightarrow \pi^*$ transitions of the 9,9-dimethyl-xanthene [37] and phenyl units. The broad band around 330 nm is characteristic of aromatic phosphines. Fife et al. [38] assigned it to an $n \rightarrow \pi^*$ transition (the excitation of an electron from the lone-pair orbital of the P atom to a π^* orbital of phenyl rings). It is more intense

than most other (e. g. carbonyl) n $\rightarrow \pi^*$ bands, which can be due partly to the coupling of this electronic transition with vibrational ones, partly to the fact that it has some $\pi \rightarrow \pi^*$ character. To distinguish it from clear n $\rightarrow \pi^*$ transitions, this transition of aromatic phosphines is frequently denoted as $\ell \rightarrow a_\pi$ (ℓone-pair $\rightarrow$ *a*nti-bonding π) [39]. In most cases, this band of diphosphine ligands is blue-shifted in the spectra of their transition metal complexes, due to the stabilization of the lone pair electrons of their P atoms, which are used for the formation of the P-metal σ bonds [40]. This shift is also shown by our complexes. In the spectrum of [$AuCl(X(CP)_2)$] solution, in which the mononuclear complex may form an equilibrium mixture with other species (see the NMR spectroscopic section), the $\sigma \rightarrow a_\pi$ transition appears as a tail on the long wavelength side of the multicomponent $\pi \rightarrow \pi^*$ band. In the spectrum of [$Au_2Cl_2(X(CP)_2)$] the band of the $\sigma \rightarrow a_\pi$ transition is not discernible, it is probably shifted completely under the $\pi \rightarrow \pi^*$ band. Theoretical calculations on two- and a three-coordinate gold(I) phosphine complexes also indicated that the HOMO-LUMO gap is expected to be larger in the two-coordinate species [41,42].

The free ligand is fluorescent in solution, with a band maximum about 390 nm, but it is not phosphorescent. The solid ligand shows a fluorescence band at a similar position. The solution sample of [$AuCl(X(CP)_2)$] shows a weak emission, which may be attributable to the free ligand. The binuclear complex, [$Au_2Cl_2(X(CP)_2)$] is non-emissive in solution.

The solid ligand as well as the solid complexes are phosphorescent. Unlike the n $\rightarrow \pi^*$ band of the ligand, which is blue shifted in the absorption spectra of the complexes, the phosphorescence band of the ligand is red shifted on coordinating the Au atom, with a larger shift in the spectrum of [$AuCl(X(CP)_2)$]. The phosphorescence lifetime increases on the coordination of the Au atoms, in particular in case of [$Au_2Cl_2(X(CP)_2$] with short Au···P and Au···Cl distances. Besides, the phosphorescence bands of the complexes have a more distinctive vibrational structure, as related to the band of the ligand.

The phosphorescence properties of gold(I) complexes are sensitive to the coordination number of the gold centers and to the presence of Au···Au interactions [43,44,45].

In the majority of the known luminescent two-coordinate Au(I) complexes the Au centers are connected by aurophilic interaction, but several luminescent two-coordinate gold(I) phosphine complexes with lack of Au···Au interaction have also been described, like [$AuCl(P(o\text{-tolyl})_3)$] [46,47], [$Au_2Cl_2$(dbfphos)] [13] (dbfphos = 4,6-bis(diphenylphosphino)dibenzofuran), [Au_2Cl_2(binap)] [23] (binap = 2,2'-bis(diphenylphosphino)-1,1'-binaphthyl) and various alkinyl gold(I) complexes with PPh_3,

PCy_3 [48] and 1,4-bis(diphenylphosphino)butane [49] auxiliary ligands. In the phosphorescence spectra of $[Au_2Cl_2(dbfphos)]$ and $[Au_2Cl_2(binap)]$, which are structurally similar to $[Au_2Cl_2(X(CP)_2]$, the position and the shape of the band are similar as in the spectra of their free ligands, indicating that the emission of these complexes originates from intra-ligand (IL) type transitions.

Three-coordinate gold(I) complexes are in general luminescent and this is not bound to the presence of aurophilic interactions [43]. In the phosphorescence spectrum of our three-coordinate complex, $[AuCl(X(CP)_2)]$, the band of the free ligand is shifted more to the red and its shape changes more markedly than in the spectrum of the two-coordinate compound, indicating that the emission of $[AuCl(X(CP)_2)]$ can not be attributed to a clear IL excited state. The emission of three-coordinate gold(I) complexes with phosphine ligands is usually assigned to metal-centered (MC) and not to IL type transitions [50]. Quantum chemical calculations on the luminescent excited states of three-coordinate gold(I) complexes with bulky phosphine ligands, like our ligand, preventing the formation of short Au···Au contacts, were carried out by Omary et al. [51,52]. It has been confirmed that the phosphorescence of $[AuL_3]^+$ complexes with L = PPh_3, $PPhCy_2$ and TPA (1,3,5-triaza-7-phosphaadamantane) ligands, arises from metal-centered (MC) transitions, whereas the emittant triplet state of $[AuCl(PPh_3)_2]$ has metal-to-ligand charge transfer (MLCT) character. Based on the similarity of the coordination of the Au atom in $[AuCl(PPh_3)_2]$ and in $[AuCl(X(CP)_2)]$, it can be presumed that the luminescence of the latter complex also arises from an MLCT state.

4. Conclusions

We have synthesized a new diphosphine, 9,9-dimethyl-4,5-bis(diphenylphosphinomethyl)-*9H*-xanthene, $X(CP)_2$, its dioxide, $X(CPO)_2$, and two gold(I) complexes of $X(CP)_2$, $[AuCl(X(CP)_2)]$ and $[Au_2Cl_2(X(CP)_2)$, and studied their structural properties using NMR spectroscopy and X-ray diffraction. Contrary to the related xantphos-type counterparts, extensive hydrogen bond network and ideal planarity of the xanthene backbone have been revealed in $X(CPO)_2$ and $[AuCl(X(CP)_2)]$. In the case of the dioxide, the planarity of the xanthene ring system has been attributed to balanced intermolecular secondary interactions affecting the two sides of the molecule. However, the same structural feature of the mononuclear complex seems to be associated with the extra conformational freedom introduced by the inserted methylene groups, which enables the Ph_2P groups to approach the gold center in the required geometry by rotating about the C(*aryl*)-C(CH_2) axes, making the bending of the xanthene backbone unnecessary. The remarkable structural

dissimilarity of $X(CPO)_2$ and $[AuCl(X(CP)_2)]$ to their xantphos-type counterparts promises fruitful further studies on this ligand and on its metal complexes more closely associated with homogeneous catalytic reactions. The results on the luminescence of the two gold complexes of $X(CP)_2$ – the long phosphorescence lifetime of $[Au_2Cl_2(X(CP)_2)]$, the strongly red-shifted phosphorescence of $[AuCl(X(CP)_2)]$ – can be helpful in the design of new organogold(I) compounds with potential organic emitter and sensor applications.

Acknowledgments

The authors wish to thank Professor Gábor Pálinkás for the fruitful discussions. The financial support from National Development Agency (Project ID: KMOP-1.1.2-07/1-2008-0002) is gratefully acknowledged.

Appendix A. Supplementary data

CCDC 890992, 890993 and 890994 contain the supplementary crystallographic data for compounds $X(CPO)_2$, **4**, $[AuCl(X(CP)_2)]$, **6**, and $[Au_2Cl_2(X(CP)_2)]$, **7**, respectively. These data can be obtained free of charge via http://www.ccdc.cam.ac.uk/conts/ retrieving.html, or from the Cambridge Crystallographic Data Centre, 12 Union Road, Cambridge CB2 1EZ, UK; fax: (+44) 1223 336 033; or e-mail: deposit@ccdc.cam.ac.uk. Further supplementary data associated with this article are presented in the Supporting Information (Tables S1-S2 and Figs. S1–S14) and can be found, in the online version, at (xxx).

References

[1] M. Kranenburg, Y. E. M. van der Burgt, P. C. J. Kamer, P. W. N. M. van Leeuwen, K. Goubitz, J. Fraanje, Organometallics 14 (1995) 3081-3089.

[2] S. Hillebrand, J. Bruckmann, C. Krueger, M. W. Haenl, Tetrahedron Lett. 36 (1995) 75-78.

[3] C. R. Landis, J. Uddin, J. Chem. Soc., Dalton Trans. (2002) 729–742.

[4] D. V. Partyka, J. B. Updegraff, M. Zeller, A. D. Hunter, T. G. Gray, Dalton Trans. (2010), 5388-5397.

[5] G. L. Williams, C. M. Parks, C. R. Smith, H. Adams, A. Haynes, A. J. H. M. Meijer, G. J. Sunley, S. Gaemers, Organometallics 30 (2011) 6166-6179.

[6] M.-N. Birkholz, Z. Freixa, P. W. N. M. van Leeuwen, Chem. Soc. Rev. 38 (2009) 1099-1118.

[7] G. Petőcz, Z. Berente, T. Kégl, L. Kollár, J. Organomet. Chem., 689 (2004) 1188-1193.

[8] A. J. Pontiggia, A. B. Chaplin, A. S. Weller, J. Organomet. Chem. 696 (2011) 2870-2876.

[9] P. C. J. Kamer, P. W. N. M. van Leeuwen, J. N. H. Reek, Acc. Chem. Res. 34 (2001) 895-904.

[10] B. Wahl, S. Giboulot, A. Mortreux, Y. Castanet, M. Sauthier, F. Liron, G. Poli, Adv. Synth. Catal. 354 (2012) 1077-1083.

[11] P. Dierkes, P. W. N. M. van Leeuwen, J. Chem. Soc., Dalton Trans. (1999) 1519-1529.

[12] M. Kranenburg, P. C. J. Kamer, P. W. N. M. van Leeuwen, Eur. J. Inorg. Chem. 1 (1998) 25-27.

[13] A. Pintado-Alba, H. de la Riva, M. Nieuwhuyzen, D. Bautista, P. R. Raithby, H. A. Sparkes, S. J. Teat, J. M. López-de-Luzuriaga, M. C. Lagunas, Dalton Trans. (2004) 3459-3467.

[14] A. Deák, T. Megyes, G. Tárkányi, P. Király, L. Biczók, G. Pálinkás, P. J. Stang, J. Am. Chem. Soc. 128 (2006) 12668-12670.

[15] G. Tárkányi, P. Király, G. Pálinkás, A. Deák, Magn. Reson. Chem. 45 (2007) 917–924.

[16] T. Tunyogi, A. Deák, Acta Cryst. C 66 (2010) m133-m166.

[17] H. Ito, T. Saito, T. Miyahara, C. Zhong, M. Sawamura, Organometallics 28 (2009) 4829-4840.

[18] R. C. Evans, P. Douglas, C. J. Winscom, Coord. Chem. Rev. 250 (2006) 2093-2126.

[19] X. He, V. W.-W. Yam, Coord. Chem. Rev. 255 (2011) 2111-2123.

[20] A. Kaltzoglou, T. F. Faessler, P. Paraskevas, J. Coord. Chem. 61 (2008) 1774-1781.

[21] C. S. Smith, C. S. Branham, B. J. Marquardt, K. R. Mann, J. Am. Chem. Soc. 132 (2010) 14079-14085.

[22] M. G. Crestani, G. F. Manbeck, W. W. Brennessel, T. M. McCormick, R. Eisenberg, Inorg. Chem. 50 (2011) 7172-7178.

[23] V. Pawlowski, H. Kunkely, A. Vogler, Inorg. Chim. Acta 357 (2004) 1309-1312.

[24] D. V. Partyka, T. S. Teets, M. Zeller, J. B. Updegraff, A. D. Hunter, T. G. Gray, Chem. Eur. J. 18, (2012) 2100-2112.

[25] V. W.-W. Yam, E. C.-C. Cheng, Chem. Soc. Rev. 37 (2008) 1806-1813.

[26] H. Schmidbaur, A. Schier, Chem Soc. Rev. 41 (2012) 370-412.

[27] K. Chibale, M. Visser, V. Yardley, S. L. Croft, A. H. Fairlamb, Bioorg. Med. Chem. Lett. 10 (2000) 1147-1150.

[28] S. A. Nagamani, Y. Norikane, N. J. Tamaoki, J. Org. Chem. 70 (2005) 9304-9313.

[29] R. El Abed, F. Aloui, J.P. Genêt, B. Ben Hassine, A. Marinetti, J. Organomet. Chem. 692 (2007) 1156-1160.

[30] F. Uson, A. Laguna, M. Laguna, Inorg. Synth. 26 (1989) 86-91.

[31] G.M. Sheldrick, Acta Cryst. A, 64 (2008) 112-122.

[32] B. Deb, D. K. Dutta, Polyhedron 28 (2009) 2258-2262.

[33] G. A. Bowmaker, J. C. Dyason, P. C. Healy, L. M. Engelhardt, C. Pakawatchai, A. H. White, J. Chem. Soc., Dalton Trans. (1987) 1089-1097.

[34] G. Szalontai, J. Bakos, I. Tóth, B. Heil, Magn. Reson. Chem. 25 (1987)761-765 .

[35] N . J. DeStefano, D. K. Johnson, R. M. Lane, L. M. Venanzi, Helv. Chim. Acta 59 (1976) 2674-2681.

[36] N. J. DeStefano, D. K. Johnson, L. M. Venanzi, Helv. Chim. Acta 59 (1976) 2691-2703.

[37] X.-Q.iZhu, Z. Dai, A. Yu, S. Wu, J.-P. Cheng, J. Phys. Chem. B 112 (2008) 11694-11707.

[38] D. J. Fife, K. W. Morse, W. M. Moore, J. Photochem. 24 (1984) 249-263.

[39] M. C. Lagunas, C. M. Fiero, A. Pintado-Alba, H. de la Riva, S. Betanzos-Lara, Gold Bull. 40 (2007) 135-141.

[40] C. Kutal, Coord. Chem. Rev. 99 (1990) 213-252.

[41] Z. Assefa, R. J. Staples, J. P. Fackler, Inorg. Chem. 33 (1994) 2790-2798.

[42] Z. Assefa, J. M. Forward, T. A. Grant, R. J. Staples, B. E. Hanson, A. A. Mohamed, J. P. Fackler, Inorg. Chim. Acta 352 (2003) 31.

[43] J. M. Forward, J. P. Fackler, Z. Assefa, in D. M. Roundhill, J. P. Fackler (Eds.) Optoelectronic Properties of Inorganic Compounds, Plenum Press, New York, 1999, pp. 195-229.

[44] J. M. Lopez-de-Luzuriaga, in A. Laguna (Ed.) Modern Supramolecular Gold Chemistry, Wiley, Weinheim, 2008, pp. 347-401.

[45] S. H. Lim, M. M. Olmstead, A. L. Balch, J. Am. Chem. Soc. 133 (2011) 10229-10238.

[46] J.-G. Kang, C. Park, E. R. T. Tiekink, Bull. Korean. Chem. Soc. 27 (2006) 299-301.

[47] E. R. T. Tiekink, J.-G. Kang, Coord. Chem. Rev. 253 (2009)1627-1648.

[48] L. Gao, D. V. Partyka, J. B. Updegraff, N. Deligonul,T. G. Gray, Eur. J. Inorg. Chem. (2009) 2711-2719.

[49] L. Rodríguez, M. Ferrer, R. Crehuet, J. Anglada J. C. Lima, Inorg. Chem. 51 (2012) 7636-7641.

[50] C. King, M. N. I. Khan, R. J. Staples, J. P. Fackler, Inorg. chem. 31 (1992) 3236.

[51] K. A. Barakat, T. R. Cundari, M. A. Omary, J. Am. Chem. Soc. 125 (2003) 14228-14229.

[52] P. Sinha, A. K. Wilson, M. A. Omary, J. Am. Chem. Soc. 127 (2005) 12488-12489.

Figure(s)
Click here to download high resolution image

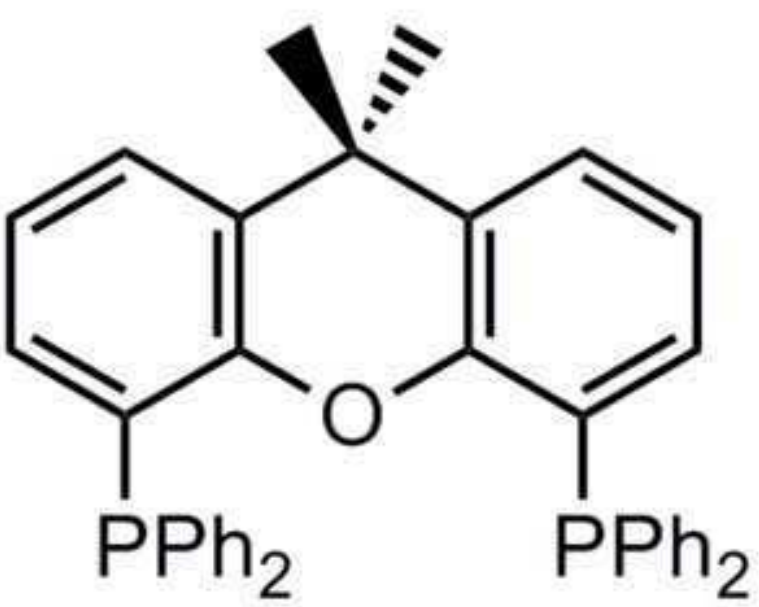

xantphos, XP_2

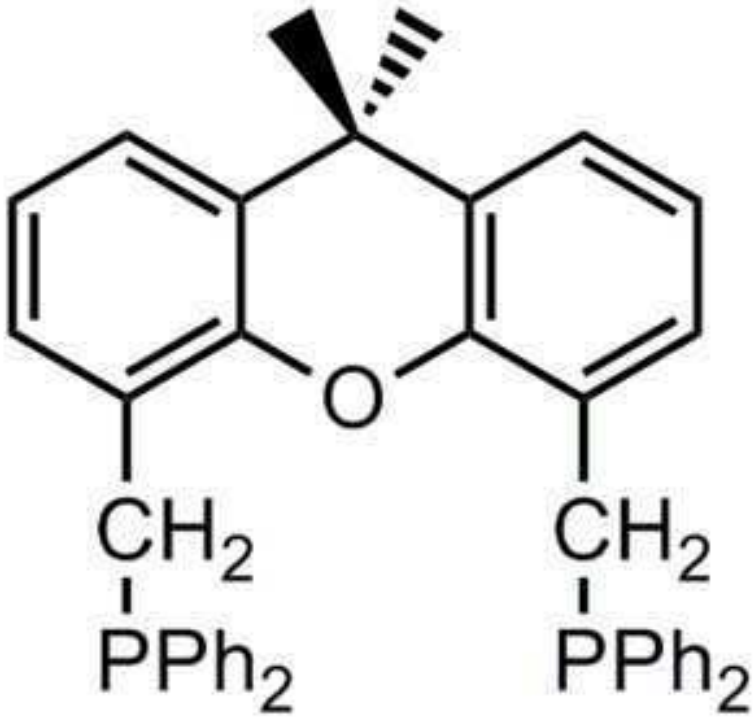

$X(CP)_2$

Scheme 1

Figure(s)
Click here to download high resolution image

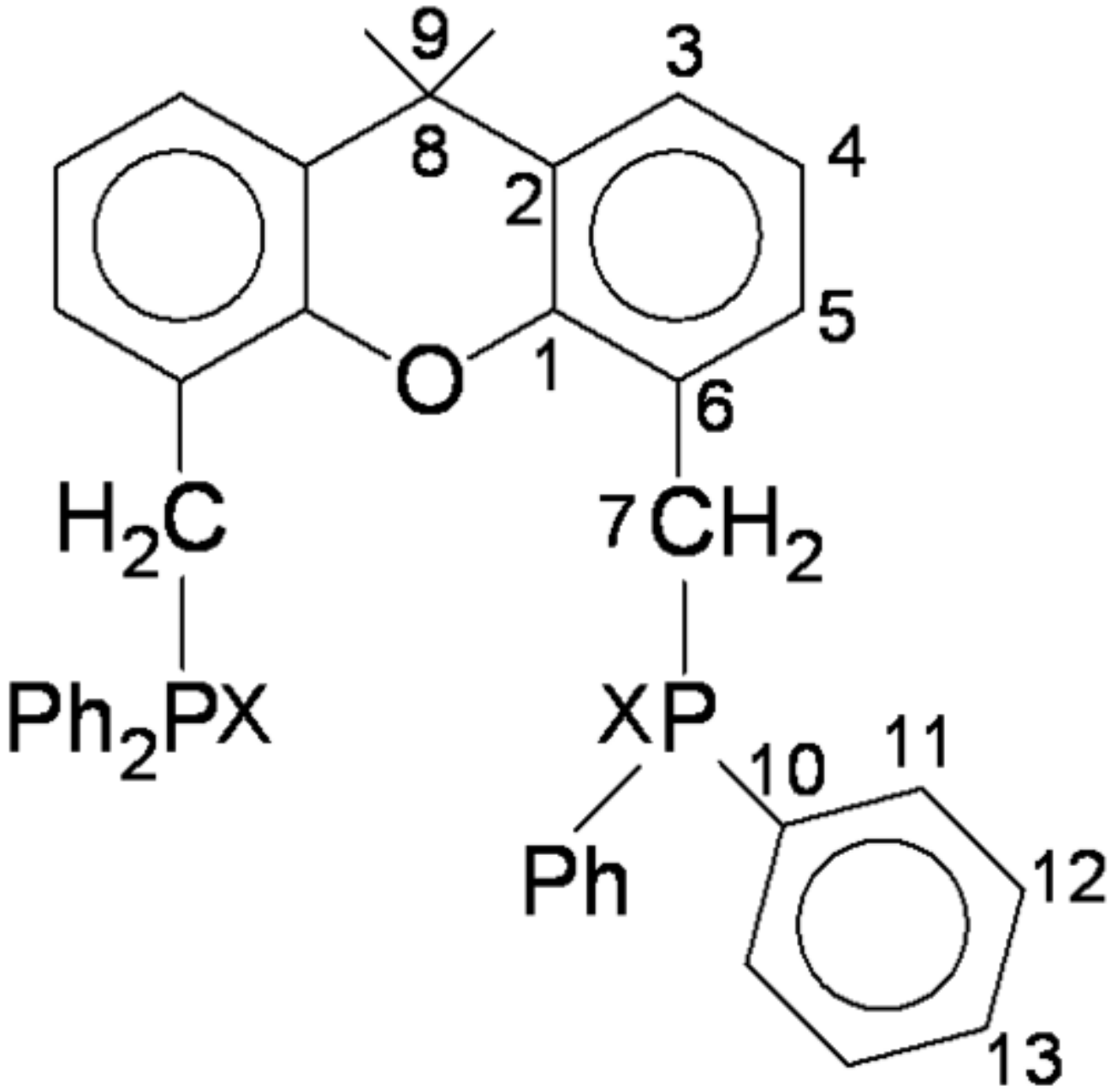

Scheme 2

Figure(s)

Click here to download high resolution image

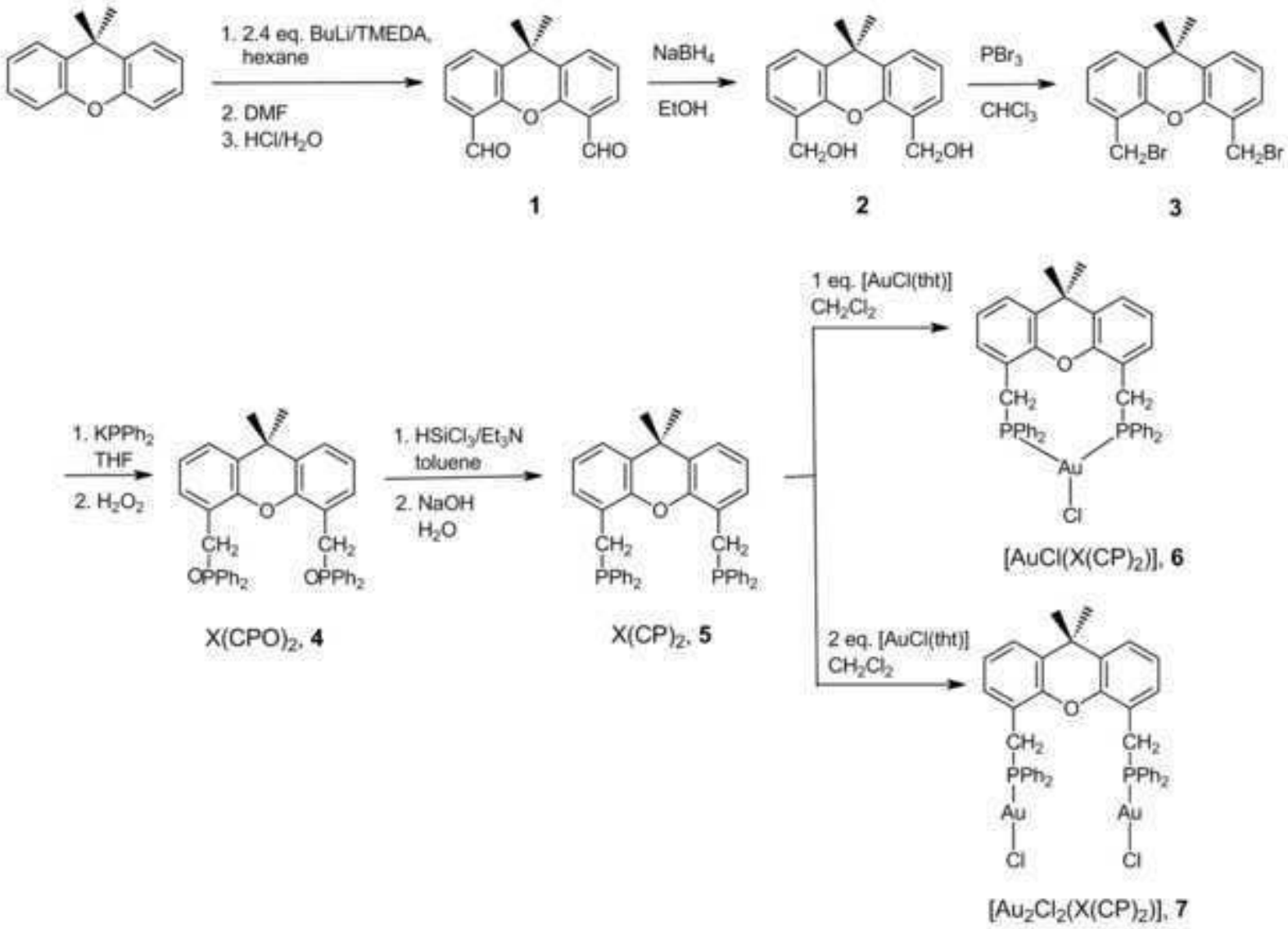

Scheme 3

Figure(s)

Captions for figures

Fig. 1. Molecular diagram of $X(CPO)_2$ with the numbering of atoms. Hydrogen atoms are omitted for clarity. Ellipsoids are drawn at the 50% probability level.

Fig. 2. A side view of $X(CPO)_2$ (left) and $X(PO)_2$ (one of the three crystallographically independent molecules) showing the symmetrical and asymmetrical arrangement of substituents of the xanthene group.

Fig. 3. Molecular diagram of $[AuCl(X(CP)_2)]$. Hydrogen atoms are omitted for clarity. Ellipsoids are drawn at the 50% probability level (left). A side view of the complex (right).

Fig. 4. Au-Cl distances (Å) *vs.* P-Au-P angles (°) for 62 gold(I) complexes

Fig. 5. Molecular diagram of $[Au_2Cl_2(X(CP)_2)]$. Ellipsoids are drawn at the 50% probability level, hydrogen atoms are omitted for clarity (left). Side view of the complex (right).

Fig. 6. (a): ^{1}H NMR spectra (400 MHz, RT, CD_2Cl_2), methylene protons only (3.74 and 4.03 ppm) and (b) ^{31}P NMR spectra (30 and 28.5 ppm) of $[AuCl(X(CP)_2)]$ (blue trace) and $[Au_2Cl_2(X(CP)_2)]$ (red trace).

Fig. 7. (a) Absorption spectra (b) phosphorescence spectra and (c) phosphorescence decay curves of $X(CP)_2$ (black trace), $[AuCl(X(CP)_2]$ (red trace) and $[Au_2Cl_2(X(CP)_2]$ (blue trace). The absorption spectra were recorded in CH_2Cl_2 solutions, $c = 5\times10^{-5}$ M. The phosphorescence spectra and decay curves were measured in solid state, setting λ_{ex} and λ_{em} to the values given under Table 4.

Figure(s)
Click here to download high resolution image

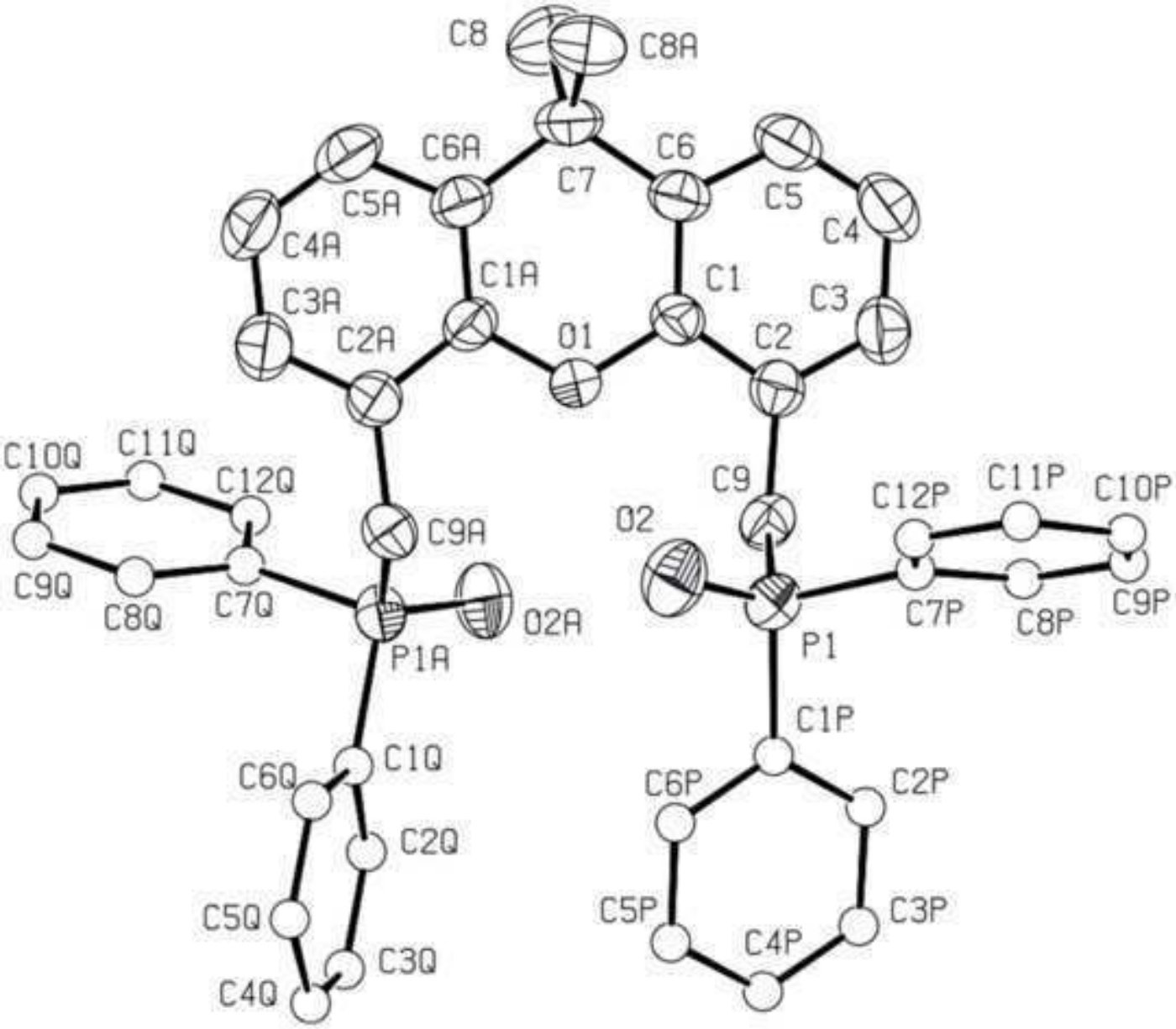

Fig. 1

Figure(s)

Click here to download high resolution image

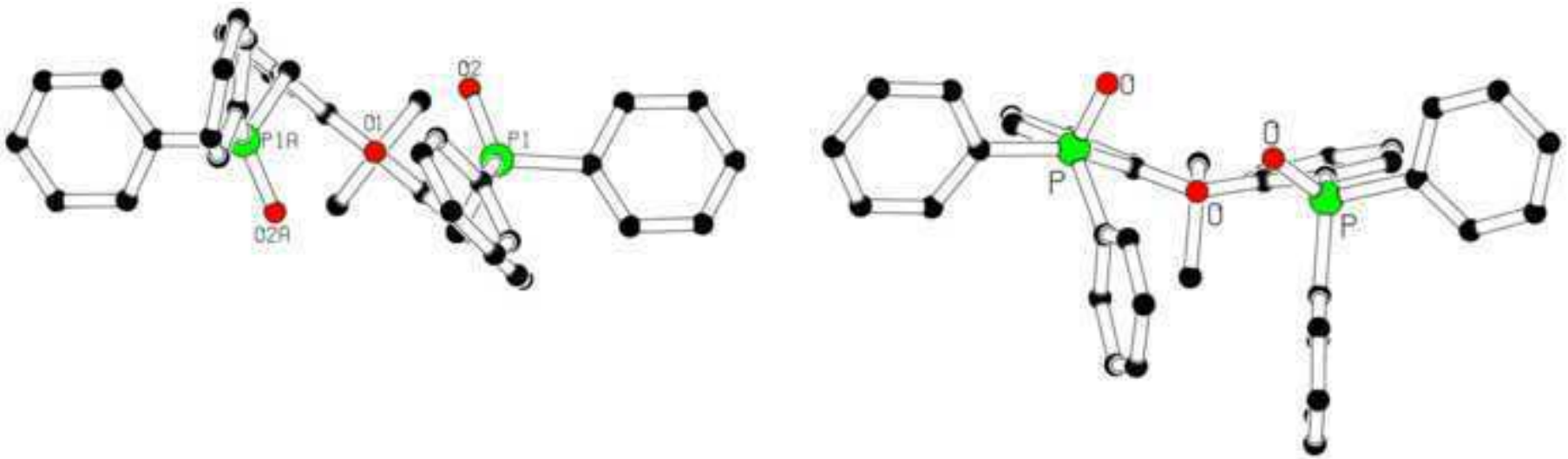

Fig. 2

Figure(s)
Click here to download high resolution image

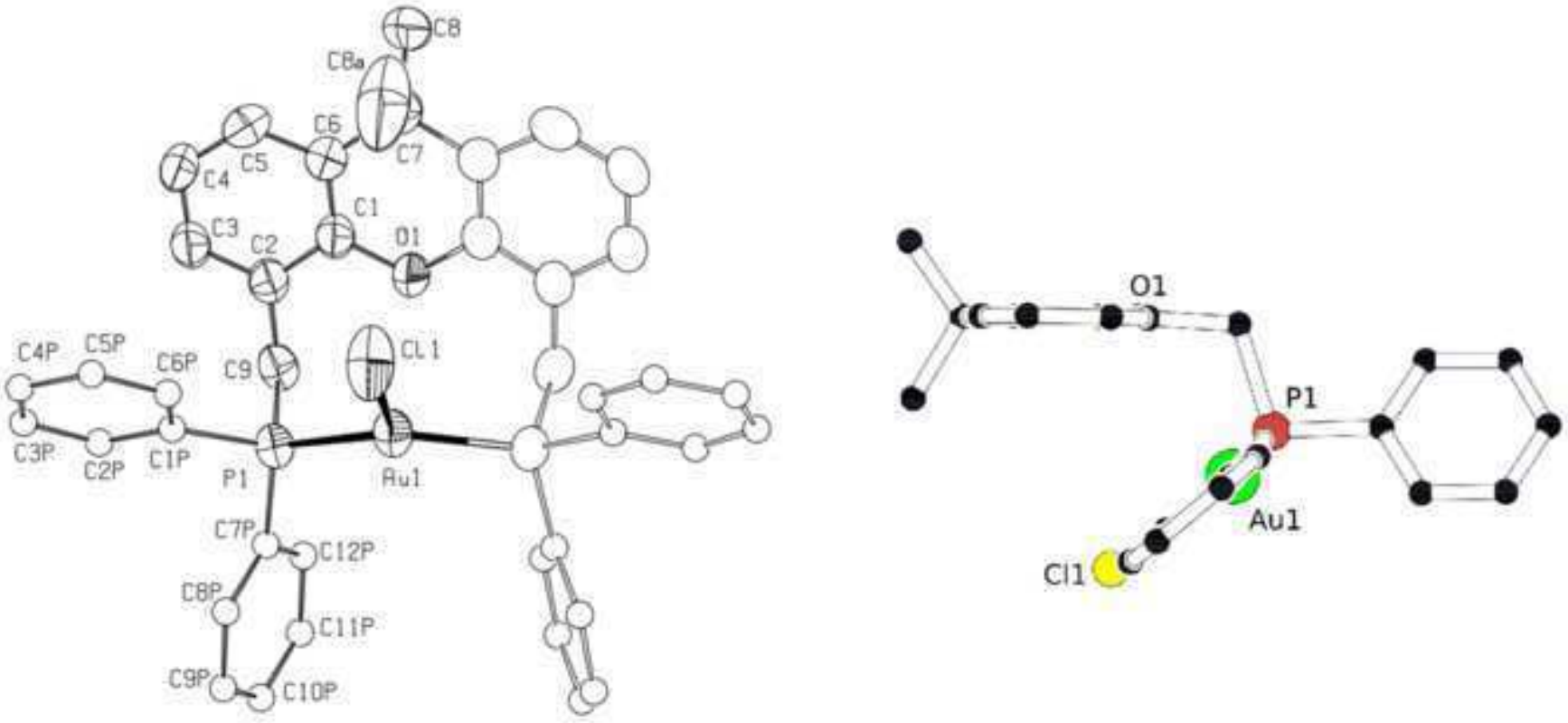

Fig. 3

Figure(s)
Click here to download high resolution image

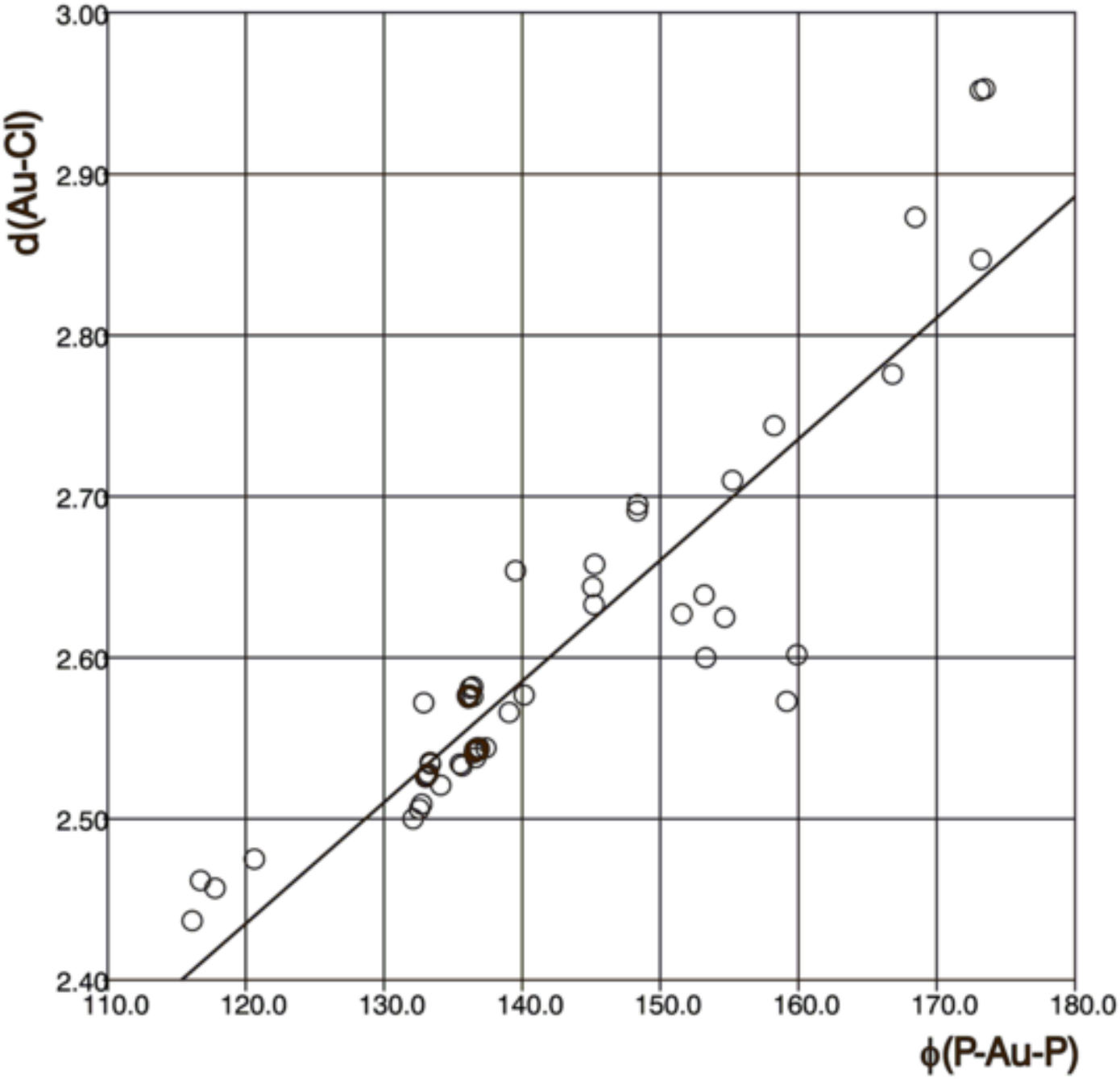

Fig. 4

Figure(s)
Click here to download high resolution image

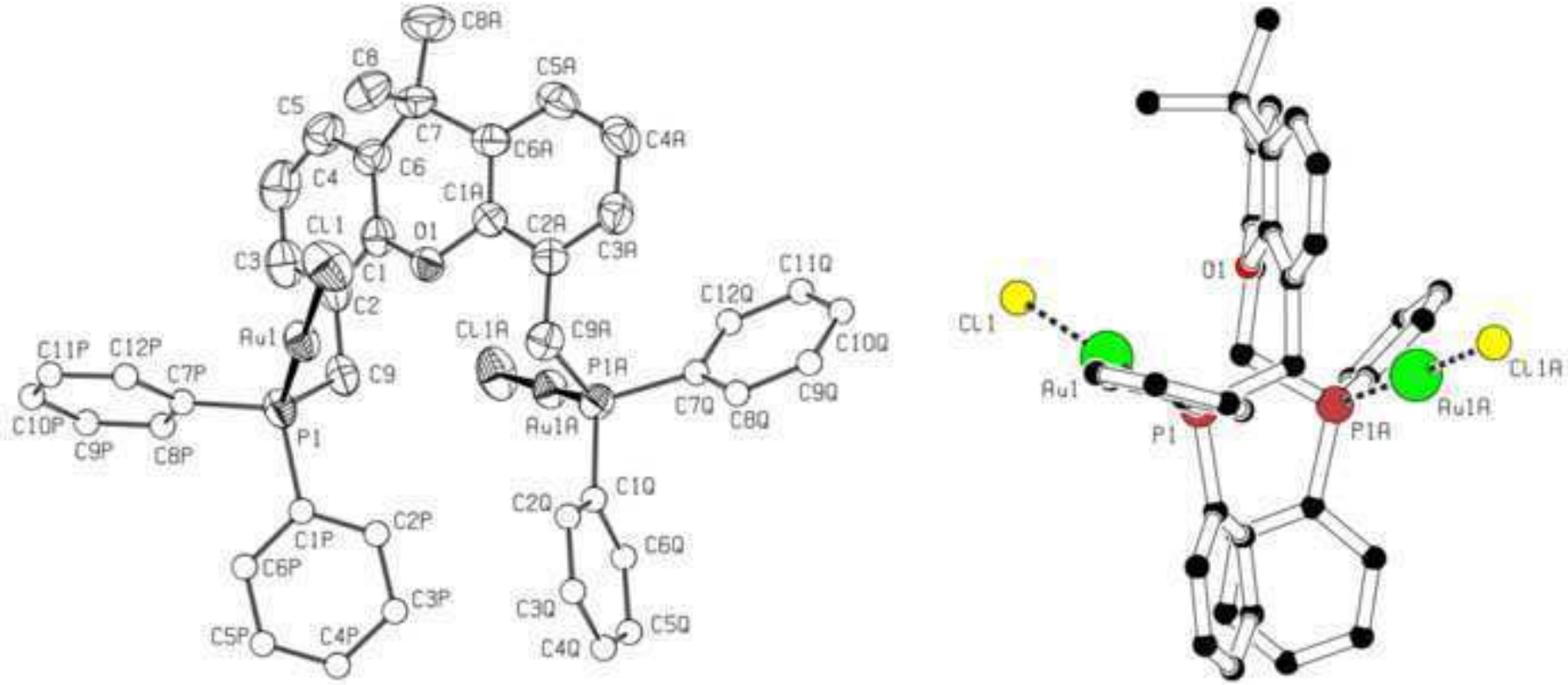

Fig. 5

Figure(s)

Click here to download high resolution image

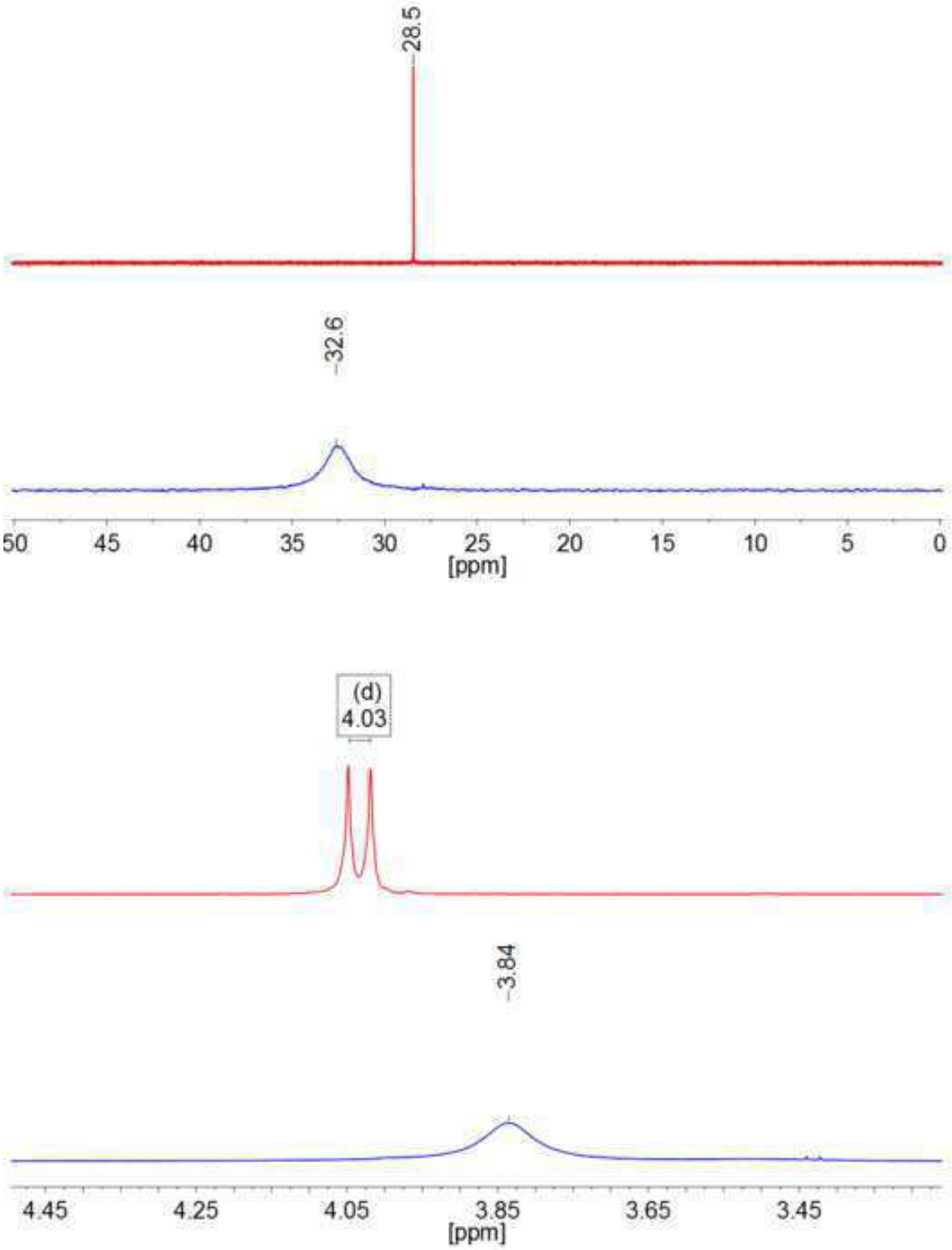

Figure(s)

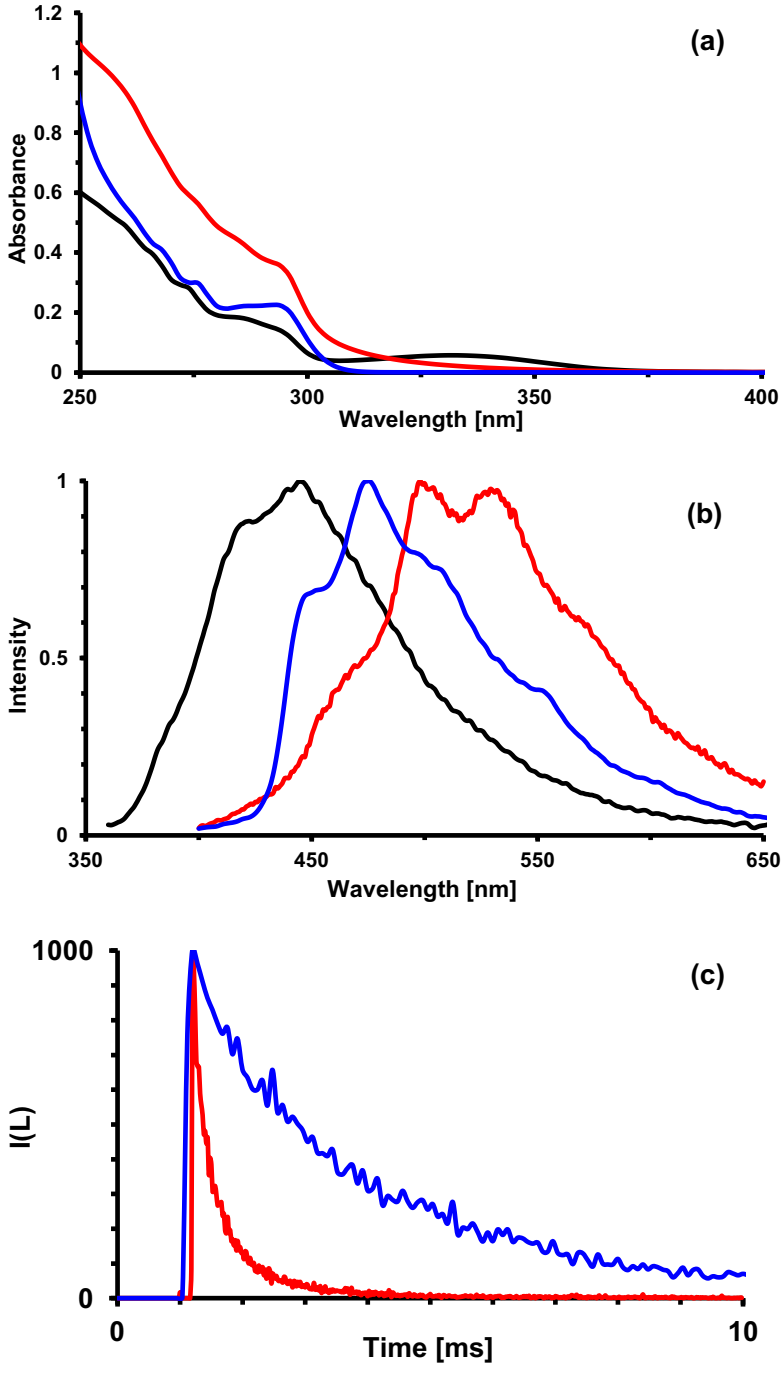

Fig. 7

Table(s)

Table 1. Crystal data, data collection and refinement parameters

		$X(CPO)_2$	$[AuCl(X(CP)_2)]$	$[Au_2Cl_2(X(CP)_2)]$
Formula		$C_{41}H_{36}O_3P_2$	$C_{41}H_{36}AuClOP_2$	$C_{41}H_{36}Au_2Cl_2OP_2$
Formula weight		638.64	839.05	1071.47
Crystal system		triclinic	orthorhombic	monoclinic
Space group		*P*-1 (No. 2)	*Pnma* (No. 62)	$P2_1/n$ (No. 14)
Unit cell	*a* [Å]	11.670(2)	12.9770(9)	11.8821(2)
	b [Å]	11.9096(15)	19.5595(15)	20.0774(4)
	c [Å]	12.801(2)	14.2934(10)	16.1880(3)
	α [°]	83.025(6)	90	90
	β [°]	71.010(6)	90	102.9818(7)
	γ [°]	86.093(6)	90	90
V [Å^3]		1669.1(4)	3628.0(5)	3763.13(12)
Z		2	4	4
D(calc) [g/cm^3]		1.271	1.536	1.891
μ(Mo-*Kα*) [mm^{-1}]		0.169	4.247	8.047
F(000)		672	1664	2048
Crystal size [mm]		0.40 x 0.52 x 0.62	0.25 x 0.51 x 0.59	0.34 x 0.38 x 0.62
θ min, max [°]		3.3, 27.5	3.1, 27.1	3.2, 28.7
Total., uniq. data, *R*(int)		79375, 7596, 0.033	32833, 4099, 0.049	134684, 9670, 0.059
Observed data [$I > 2.0\ \sigma(I)$]		6235	3185	8173
Nref, Npar		7596, 417	4099, 236	9670, 432
R, wR2, S		0.0442, 0.1280, 1.06	0.0328, 0.0716, 1.14	0.0322, 0.0616, 0.99

Table 2. Strong non-classical hydrogen bond interactions (D = donor, A = acceptor).

D-H	A	D-H (Å)	H···A (Å)	D···A (Å)	D-H···A (°)
		$X(CPO)_2$			
C9a-H9ab	O2	0.93	2.54	3.512(2)	176
C2p-H2p	O2a [1-*x*,-*y*,1-*z*]	0.93	2.57	3.405(3)	149
C6p-H6p	O2	0.93	2.56	2.980(3)	108
C6q-H6q	O2 [1-*x*,1-*y*,1-*z*]	0.93	2.39	3.212(3)	148
C8p-H8p	O2a [1-*x*,-*y*,1-*z*]	0.93	2.56	3.489(2)	176
C12p-H12p	O2	0.93	2.55	2.979(3)	109
		$[AuCl(X(CP)_2)]$			
C6p-H6p	Cl1	0.93	2.72	3.640(4)	171
C12p-H12p	Cl1[1/2+*x*,1/2-*y*,3/2-*z*]	0.93	2.75	3.622(6)	156
		$[Au_2Cl_2(X(CP)_2)]$			
C9a-H9d	O1	0.97	2.41	2.806(6)	104

Table 3. The geometry around the Au atom (Å and °)

	[AuCl(X(CP)$_2$)]	[Au$_2$Cl$_2$(X(CP)$_2$)]	[Au$_2$Cl$_2$(XP$_2$)][a]
Au1-Cl1	2.523(2)	2.282(1)	2.301(2)
Au1a-Cl1a		2.286(1)	2.307(2)
Au1-P1	2.306(1)	2.232(1)	2.235(2)
Au1-P1a	2.306(1)		
Au1a-P1a		2.231(1)	2.241(2)
Au···Au			2.9947(4)
Au1···O1	3.056(4)	3.136(3)	3.10
Au1a···O1		3.577(3)	3.99
Cl1-Au1-P1	114.57(3)	176.27(5)	173.07(6)
Cl1-Au1-P1a	114.57(3)		
Cl1a-Au1a-P1a		177.20(5)	168.47(7)
P1-Au1-P1a	129.49(4)		
P1-Au1···O1	81.5(2)	82.0(3)	65.3
P1a-Au1a···O1		77.7(3)	48.9
P1a-Au1..O1	81.5(2)		

[a] from Ref. [13]

Supporting Information

Title: A New Xantphos-type Ligand and its Gold(I) Complexes: Synthesis, Structure, Luminescence

Authors: Gábor Besenyei, István Bitter, László Párkányi, Gábor Szalontai, Péter Baranyai, Éva Kunsági-Máté, Ferenc Faigl, Alajos Grün, Miklós Kubinyi*

Table S1. Selected bond lengths (Å) and angles (°) for $X(CPO)_2$

P1-O2	1.483(1)	P1a-O2a	1.487(1)
P1-C1p	1.810(2)	P1a-C1q	1.809(2)
P1-C7p	1.812(2)	P1a-C7q	1.807(2)
P1-C9	1.812(2)	P1a-C9a	1.818(2)
O2-P1-C7p	111.18(9)	C1q-P1a-C9a	105.45(7)
O2-P1-C9	115.86(8)	C7q-P1a-C9a	105.90(8)
C1p-P1-C7p	107.64(8)	O2a-P1a-C1q	112.68(8)
C1p-P1-C9	103.43(8)	O2a-P1a-C7q	111.24(8)
C7p-P1-C9	107.28(8)	O2a-P1a-C9a	115.82(8)

Table S2. Short ($\Delta \leq -0.20$ Å) contact distances (d), the corresponding sum of van der Waals radii (R_{vdw}) and their differences (Δ) (Å)

	d	$\Sigma(R_{vdw})$	Δ
[AuCl(X(CP)$_2$)]			
Cl1...H6p	2.72	2.95	-0.23
Cl1...H12p[-1/2+x,1/2-y,3/2-z]	2.75	2.95	-0.20
Cl1...H12p[-1/2+x,y,3/2-z]	2.75	2.95	-0.20
Cl1...H6p[x,1/2-y,z]	3.056(4)	3.82	-0.76
O1...H9a	2.46	2.72	-0.26
O1...H9a[x,1/2-y,z]	2.46	2.72	-0.26
[Au$_2$Cl$_2$(X(CP)$_2$)]			
C5a...H8ab	2.70	2.90	-0.20
C7p...H6p	2.68	2.90	-0.22
C8a...H5	2.60	2.90	-0.30
C8a...H5a	2.61	2.90	-0.29
C9a...H2q	2.70	2.90	-0.20
H8aa...H5	2.17	2.40	-0.23
H8ab...C5a	2.70	2.90	-0.20
H8ab...H5a	2.14	2.40	-0.26
H2q...C9a	2.70	2.90	-0.20
H5...C8a	2.60	2.90	-0.30
H5...H8aa	2.17	2.40	-0.23
H5a...C8a	2.61	2.90	-0.29
H5a...H8ab	2.14	2.40	-0.26
H6p...C7p	2.68	2.90	-0.22
H9b...O1	2.49	2.72	-0.23
H9d...O1	2.41	2.72	-0.31

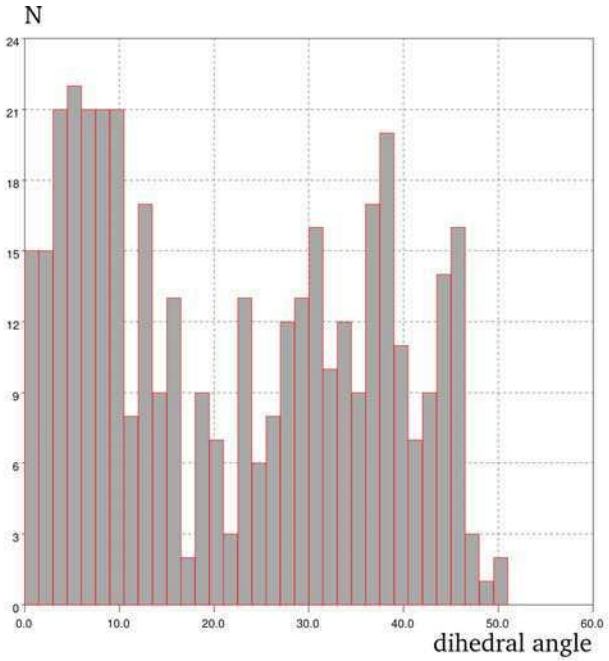

Figure S1. Distribution of dihedral angles made by the phenyl rings in reported xanthene moieties (mean: 22.0°).

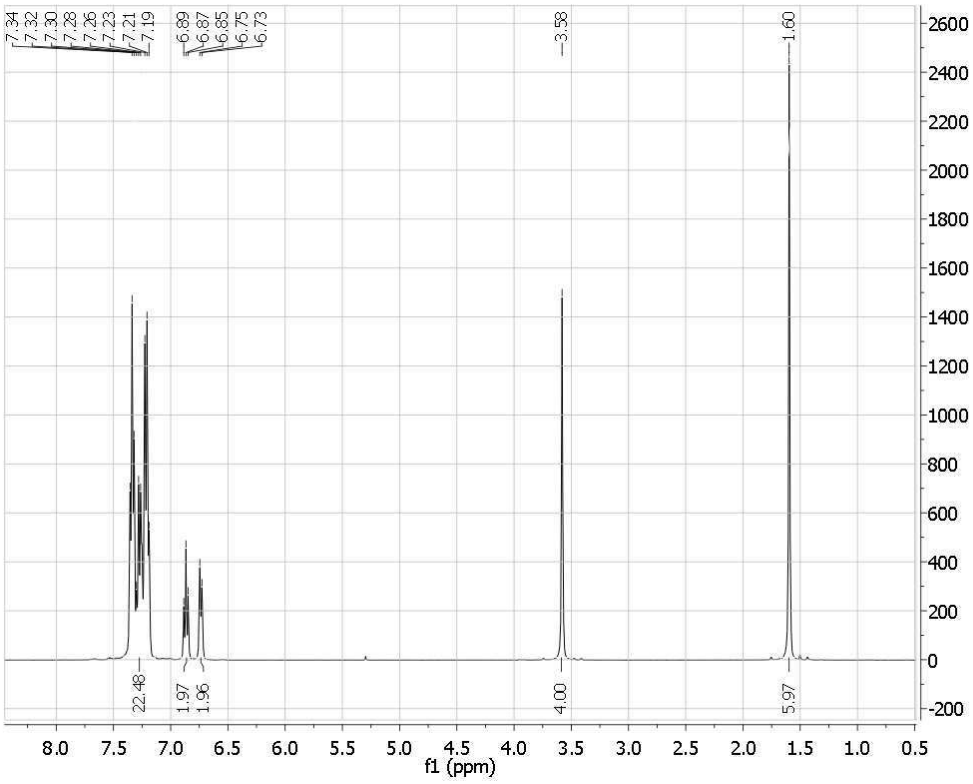

Figure S2. ^{1}H NMR spectrum of $X(CP)_2$.

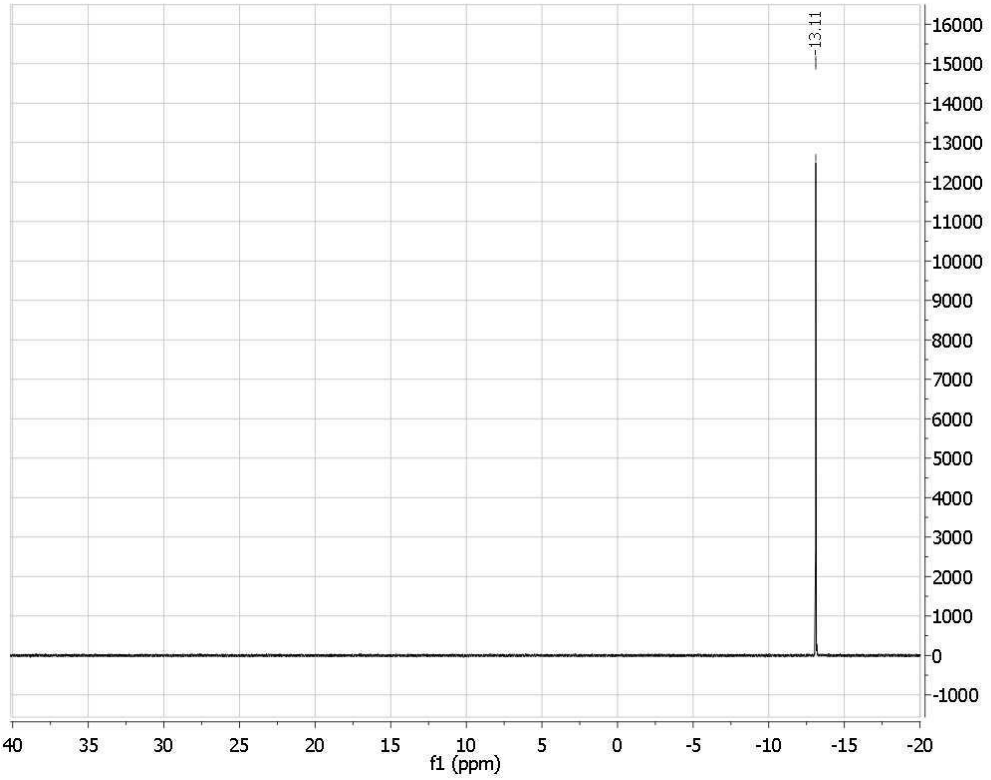

Figure S3. ^{31}P NMR spectrum of $X(CP)_2$.

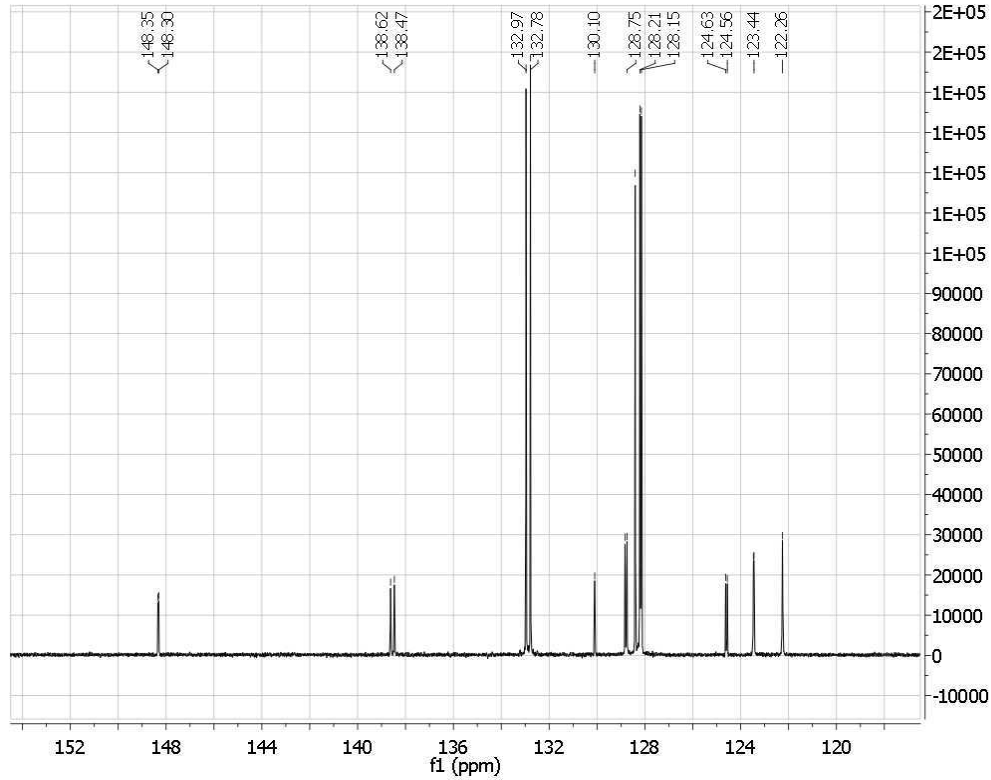

Figure S4. ^{13}C NMR spectrum of $X(CP)_2$ (section of aromatic carbon atoms).

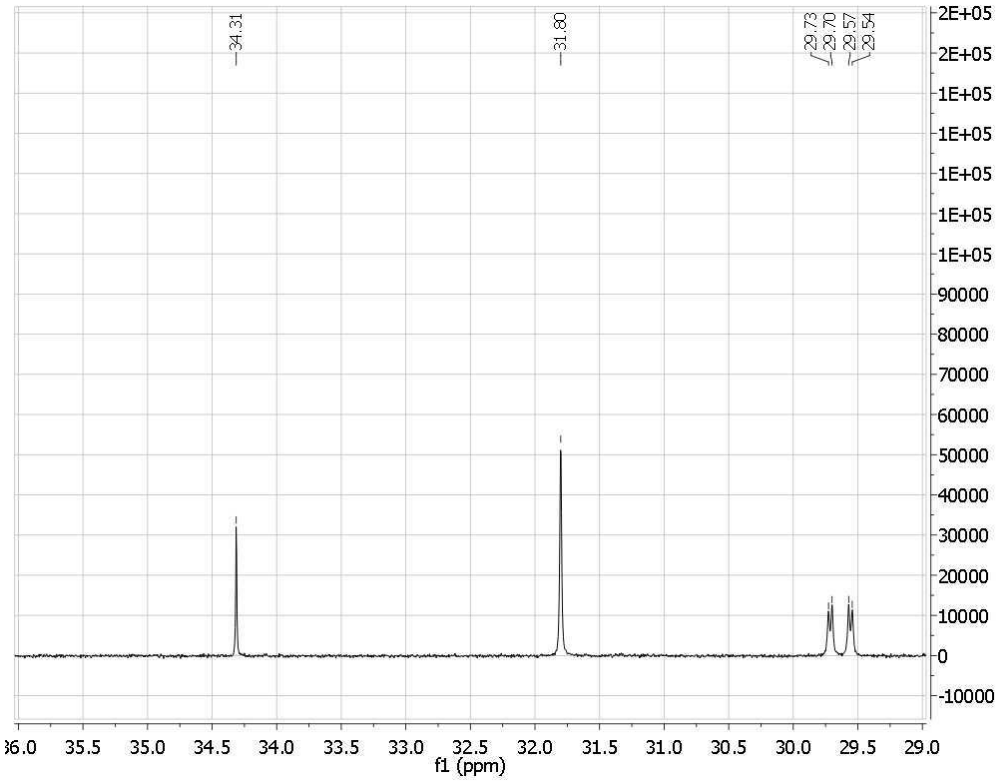

Figure S5. ^{13}C NMR spectrum of $X(CP)_2$ (section of aliphatic carbon atoms).

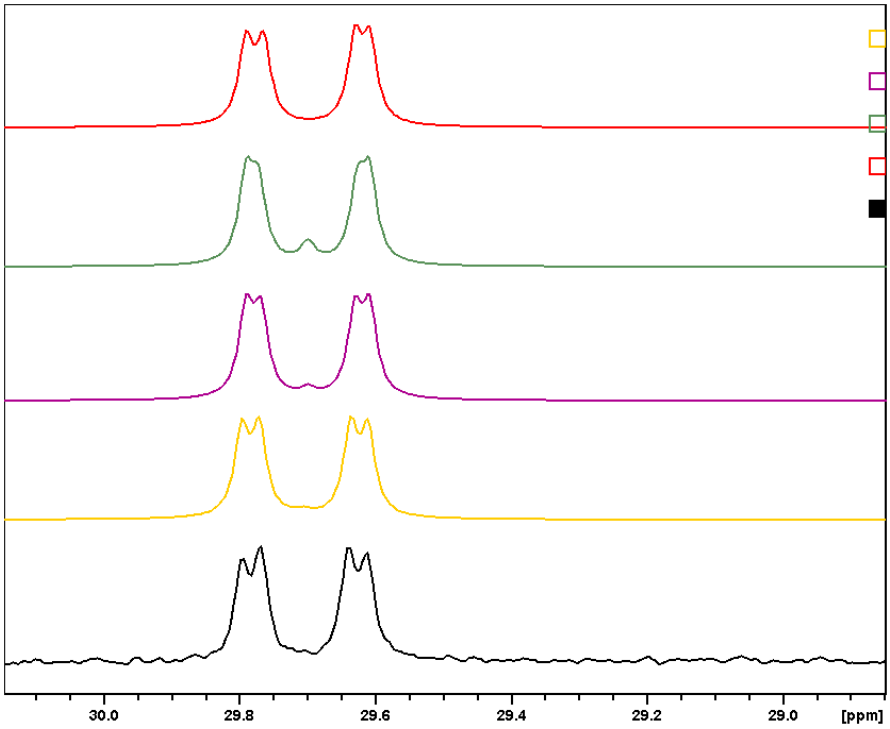

Figure S6. Simulations (colored) and experimental (black) data of carbon 7 (AXX' spin system, A = C-13, X, X'= P-31). The yellow curve was obtained by assuming J(AX)=16 Hz, J(AX')= -2.5 Hz and J(XX')= +/- 1.6 Hz coupling values. Red curve: J(XX')= 0 Hz.

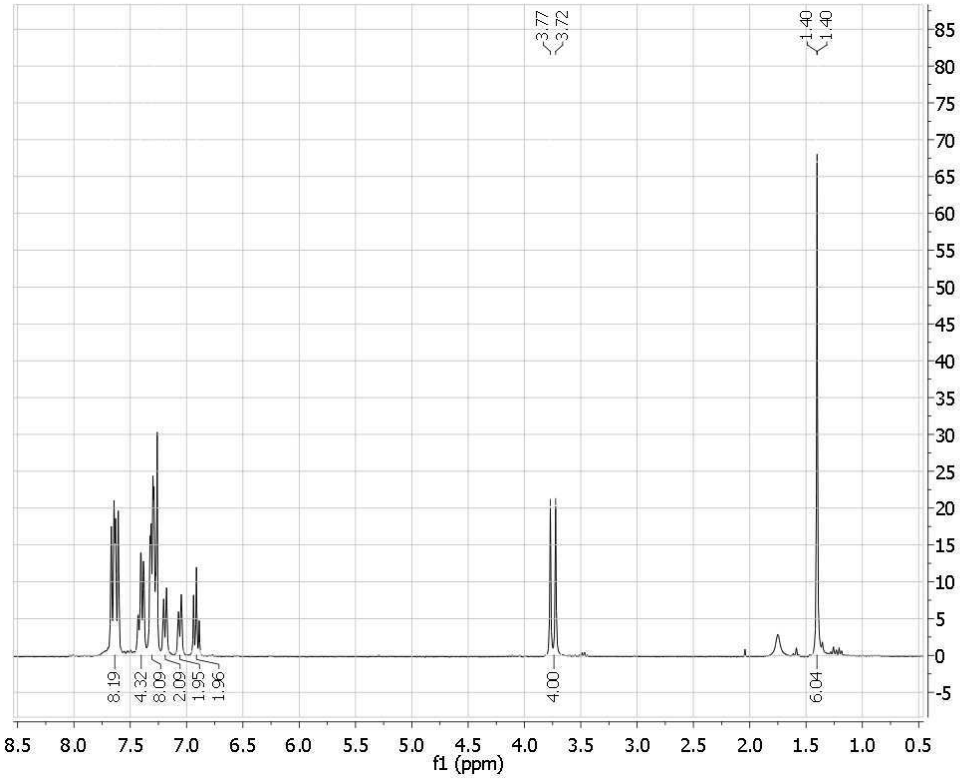

Figure S7. ^{1}H NMR spectrum of $X(CPO)_2$.

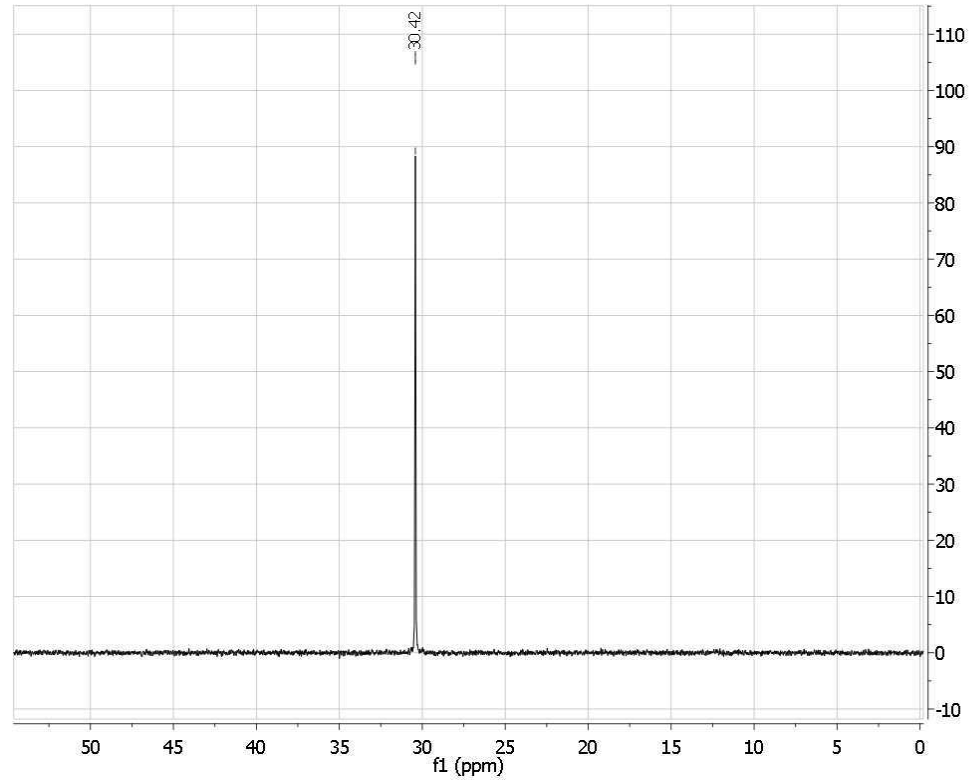

Figure S8. ^{31}P NMR spectrum of $X(CPO)_2$.

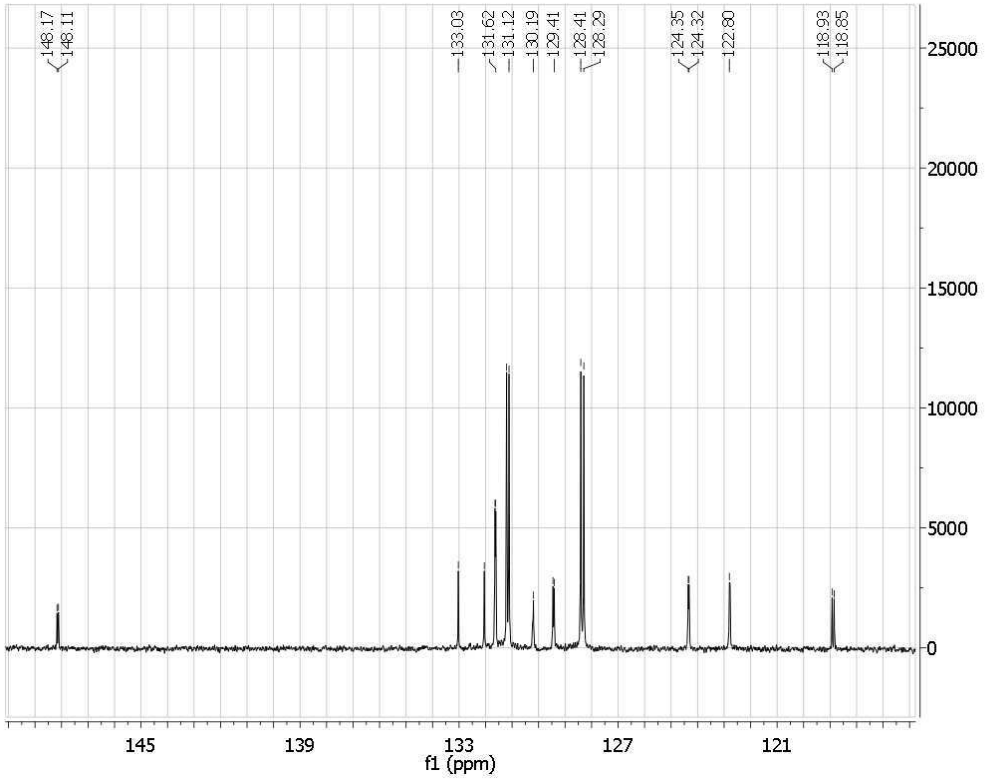

Figure S9. ^{13}C NMR spectrum of $X(CPO)_2$ (section of aromatic carbon atoms).

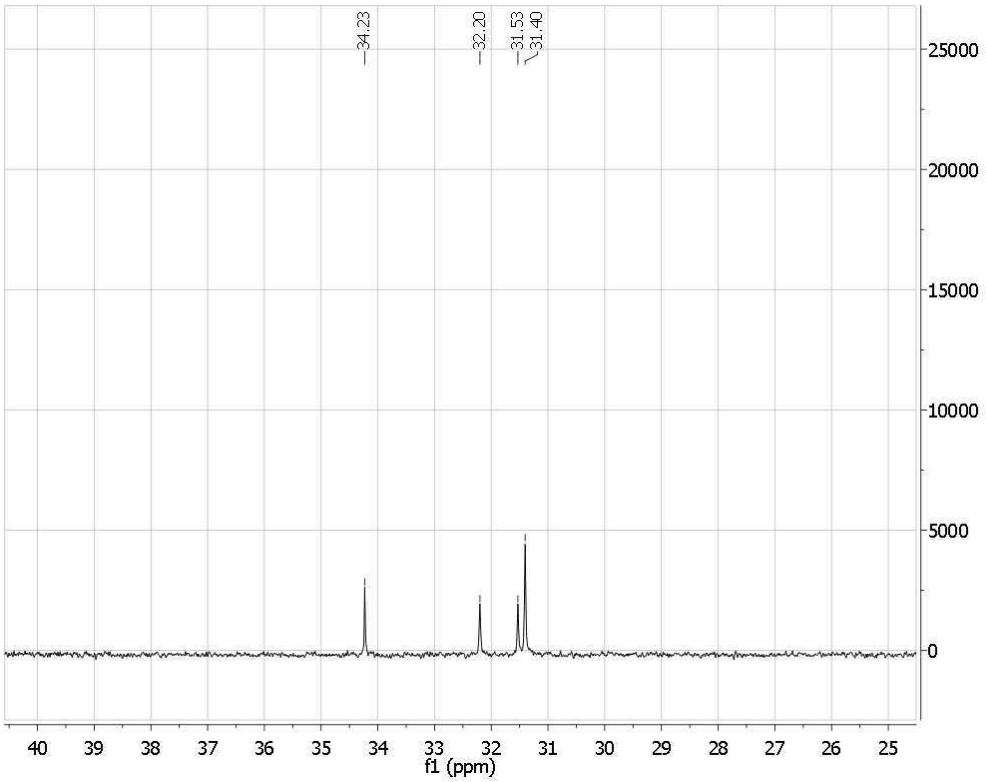

Figure S10. ^{13}C NMR spectrum of $X(CPO)_2$ (section of aliphatic carbon atoms).

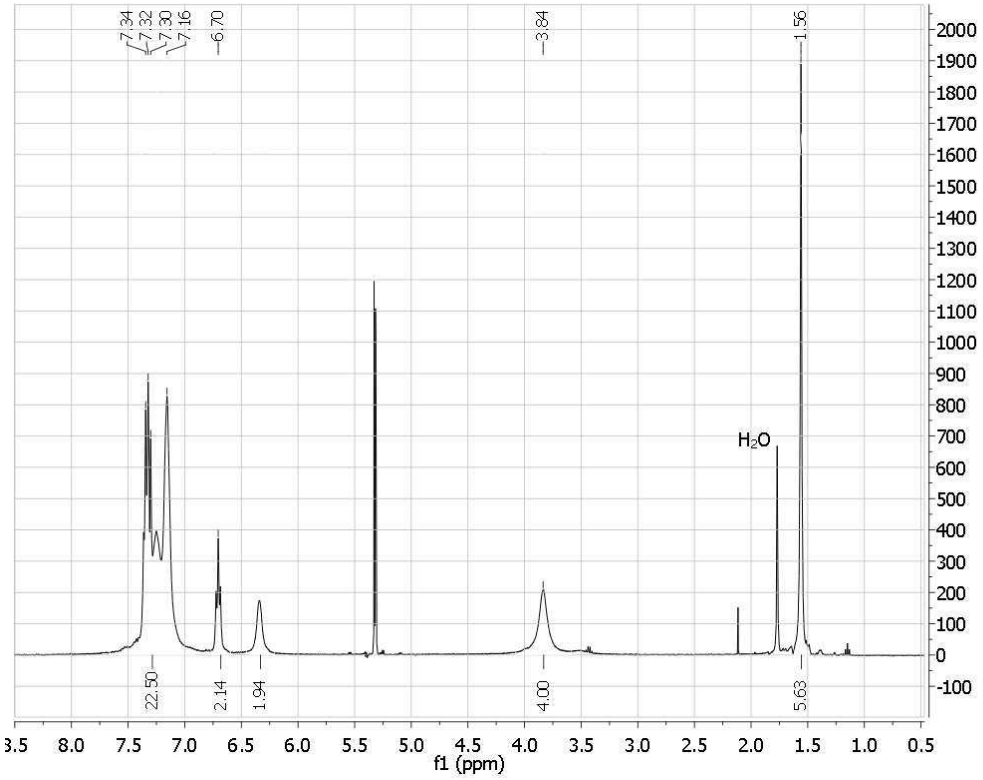

Figure S11. ^{1}H NMR spectrum of the monogold complex [AuCl(X(CP)$_2$)].

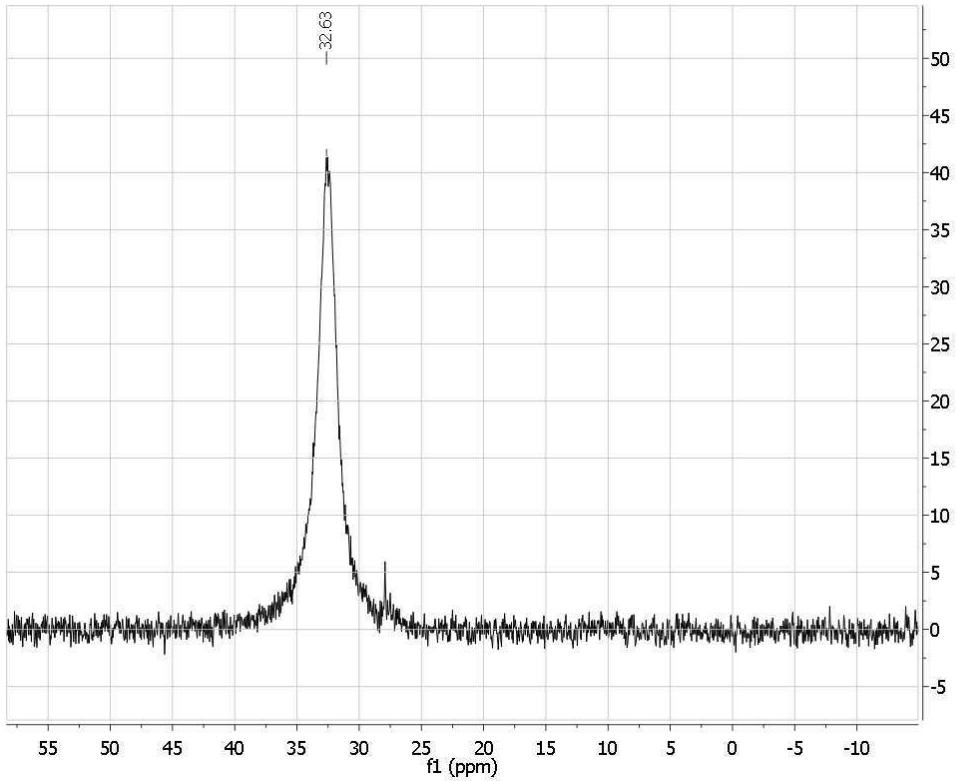

Figure S12. ^{31}P NMR spectrum of the monogold complex [AuCl(X(CP)$_2$)].

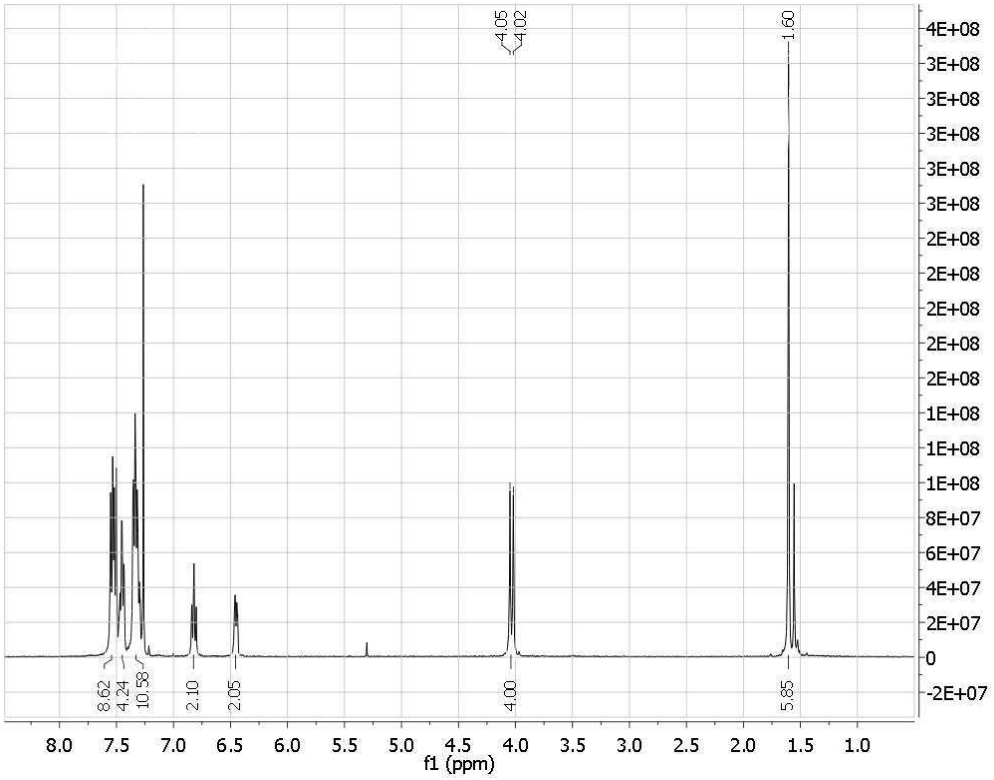

Figure S13. ^{1}H NMR spectrum of the digold complex $[Au_2Cl_2(X(CP)_2)]$.

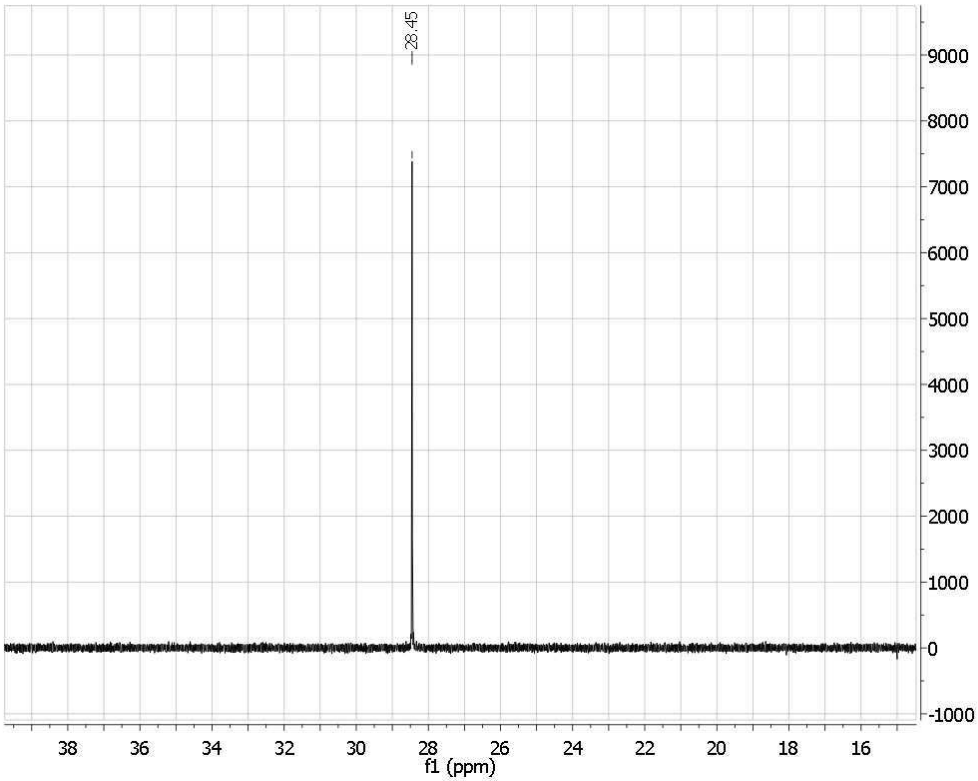

Figure S14. ^{31}P NMR spectrum of the monogold complex $[Au_2Cl_2(X(CP)_2)]$.